



**Taking Nanotechnological Remediation Processes
from Lab Scale to End User Applications
for the Restoration of a Clean Environment**

Project Nr.: 309517
EU, 7th FP, NMP.2012.1.2

**WP7: Modelling Tool for Nanoparticle Mobility
and Interaction with Contaminants**

**D7.2 Simulation Module for Predicting Transport
of NPs in Groundwater**

Tiziana Tosco, Carlo Bianco, Rajandrea Sethi (POLITO);
Pauline van Gaans, Johan Valstar, Asako Fujisaki, Amir Raof,
Majid Hassanizadeh (Deltares)



8 December 2016



[Downloaded from www.nanorem.eu/toolbox](http://www.nanorem.eu/toolbox)

The research leading to these results has received funding from the
European Union Seventh Framework Programme (FP7/2007-2013)
under Grant Agreement n° 309517

List of co-authors:

Name, First Name	Partner Organisation
Tiziana Tosco, Carlo Bianco, Rajandrea Sethi	Politecnico di Torino
	
Pauline van Gaans, Johan Valstar Asako Fujisaki, Amir Raoof, Majid Hassanizadeh	Stichting Deltares
	

This DL was submitted to the PAG members for review, specifically:

Name, First Name	Partner Organisation
Mark Wiesner	DUKE University
Pierre Matz	Solvay
Mengfang Chen	Chinese Academy of Sciences

Reviewed and agreed by PMG

Table of Contents

List of Figures	iv
List of Tables	v
Summary	1
1 Introduction	2
1.1 <i>NanoRem WP7: Modelling tool for nanoparticle mobility and interaction with contaminants</i>	2
1.2 <i>This Deliverable</i>	2
2 Pore-scale modelling	4
2.1 <i>Models and tools developed</i>	4
2.1.1 The NanoPNM model	4
2.1.2 Pre- and post-processing tools for NanoPNM	4
2.1.3 Optimization tool for NanoPNM setup	8
2.2 <i>Model results and conclusions drawn</i>	8
2.2.1 Tracer flow	8
2.2.2 Nanoparticle breakthrough	9
2.2.3 Conclusions on NP transport	14
3 Macro-scale modelling	16
3.1 <i>Mechanisms controlling particle transport in porous media</i>	16
3.2 <i>Models and functionality developed</i>	18
3.2.1 MNMs for 1D modelling of NP transport.....	18
3.2.2 Functionality of MNMs	19
3.2.3 MNM3D for 3D NP transport modelling	21
3.3 <i>Model validation</i>	22
3.4 <i>Discussion and conclusions</i>	24
4 Using the modelling tools to assist NP-based remediation	26
4.1 <i>Getting the software</i>	26
4.2 <i>Limiting the number of tests to be performed in the laboratory</i>	26
4.3 <i>Exploring different implementation scenarios</i>	26
4.4 <i>Guiding monitoring and testing assumptions</i>	27
4.5 <i>Overall strategy</i>	27
5 Large scale modelling results	30
5.1 <i>Carbo-Iron® injection in the small flume experiment</i>	30
5.2 <i>Carbo-Iron® injection in the large scale flume experiment</i>	31
5.3 <i>Carbo-Iron® injection at Balassagyarmat</i>	35
6 Conclusions	39
6.1 <i>Pore scale modelling</i>	39
6.2 <i>Macro scale modelling</i>	39
List of References	41

List of Figures

Figure 1:	NanoRem WP7 in a nutshell.....	3
Figure 2:	The 26 possible pore throats (pipes) for central pore nr. 14 in 3-dimensions (Raouf and Hassanizadeh, 2010). Numbers in a box represent the direction number 1-13.	4
Figure 3:	Flowchart of NanoPNM pre-processing.....	6
Figure 4:	Flowchart of NanoPNM post-processing.....	7
Figure 5:	Breakthrough curve data from the pore network model and the fitted upscaled model for a tracer (green, top) and a hypothetical NP (blue, bottom) for a situation with limited adsorption of NP (example 1 of Table 4).....	11
Figure 6:	Breakthrough curve data from the pore network model and the fitted upscaled model for a tracer (green) and a hypothetical NP model (blue) for a situation with strong adsorption of NP (example 2 of Table 4).....	12
Figure 7:	Attachment and detachment rates for the individual pore throats in the NanoPNM pore network model and the effective values of the fitted upscaled model for example 2 of Table 4. The inset shows the same data using logarithmic axis-scales.....	12
Figure 8:	Histograms of attachment rates (left) and detachment rates (right) in the pore network model.....	13
Figure 9:	Experimental and macro scale modelled breakthrough curves for the Carbo-Iron® column experiment; left using water type F.I.s; right using water type F.I.h.....	14
Figure 10:	Pore scale particle retention processes; d_{50} is median grain size of the PM; x is distance travelled in the PM domain from the inlet point; β , A , B are fitting parameters. Modified from Tosco et al. (2014b).	16
Figure 11:	Structure and main features of MNMs.....	18
Figure 12:	Transport model run in predictive or inverse mode.....	19
Figure 13:	The MNMs graphical interface: (a) DLVO interaction profile calculation; (b) single collector efficiency calculation; (c) particle transport simulation under transient ionic strength conditions.....	21
Figure 14:	Radial geometry: conceptual model and example of simulation results [modified from Tosco et al. (2014a)].	21
Figure 15:	MNM3D validation versus experimental data (dots) and MNMs simulation results. Interpretation of a column test of ferrihydrite nanoparticle (blue solid line for MNM3D and red dashed line for MNMs) transport under transient ionic strength conditions. Ionic strength (purple solid line for MNM3D and cyan dashed line for MNMs) varies from 5mM during the particle injection to 0.1 mM during flushing with freshwater. Experimental data from Tosco et al. (2012).	23
Figure 16:	a) Conceptual model of the simulation domains used in MNMs (2D radial) and MNM3D (full 3D). b) MNM3D validation against MNMs simulation results. Injection of micro- and nanoparticles (particle diameter of 1200 nm, 800 nm and 80 nm) through a well having a diameter of 25 cm.	24
Figure 17:	Procedure for the interpretation of column transport tests to derive information for the simulation at larger scales.....	28
Figure 18:	Front view of the large scale flume. Experimental setup (A) and model (B).....	30
Figure 19:	Spreading area of Carbo-Iron® concentration (front view, experiment carried out at VEGAS) after 7 (A) and 34 (B) minutes from the start of the particle injection. Visual comparison	

between experimental (black plume) and simulated (colored) results of nanoparticle transport (C, D) and tracer transport (E, F) (Bianco et al. 2016).	31
Figure 20: Conceptual model of the Large Scale Flume Experiment.....	32
Figure 21: Visual analysis of the Carbo-Iron® plume through the glass wall of the tank.....	32
Figure 22: Simulation of Carbo-Iron® injection in the large scale flume: vertical section. The injection well is located at $x = 2.5$ m from the left of the tank. The section A-A indicates the distance from the bottom of the tank at which the simulation results and the core sample analysis are compared in Figure 25.	33
Figure 23: Cascading column test: a) schematic representation of the test; b) and c) fitting of the breakthrough curves obtained by measuring the outlet concentration of the first and second column respectively	33
Figure 24: Simulation of Carbo-Iron® injection (view from the top) and position of the core sampling. Zoom on the injection area at 1.3 m from the bottom of the tank.	34
Figure 25: Location of injection (I-1, I-2, I-3) and monitoring points (CMT-7, CMT-8, CMT-9)	36
Figure 26: Large scale model (section view) of the Balassagyarmat site provided by Golder before the refinement of the grid as required for NP transport simulation. Green represents the high permeability layer where NPs were injected.	36
Figure 27: Interpretation of Carbo-Iron® transport test using MNMs. Experimental data from UFZ.....	37
Figure 28: MNM3D simulation of Carbo-Iron® concentration after 9 h of injection at 25 l/min.....	38

List of Tables

Table 1: Regression equations for hydraulic parameters	8
Table 2: Parameters used in the equations for attachment and detachment rates at the single pore scale.....	9
Table 3: Equations for the rate of attachment and detachment at the scale of (i.e. averaged over) a single pore. For the explanation of the parameters used see Table 2.	10
Table 4: Input and derived parameters for pore network model and fitted parameters for upscaled model for two typical examples	10
Table 5: Comparison of the ratio of the parameters for the two water types for both fitted experimental data and the upscaling equations	14
Table 6: Software comparison: Stanmod, Hydrus-1D and MNMs	19
Table 7: Properties of the setup and operating conditions of the cascading column experiment carried out at VEGAS	34
Table 8: Comparison of measured (derived from TOC analysis) and simulated concentration at the core sampling points at a distance of 1.3 m from the bottom of the tank.	35
Table 9: TOC analyses of soil samples from field site for estimation of particle fate	35
Table 10: Kinetic coefficients estimated by Carbo-Iron® column test carried out by UFZ. Porous medium from core samples from the Balassagyarmat site.....	37

Summary

Nanoparticles (NPs) used in groundwater remediation are typically delivered to the contaminated area dispersed in water-based slurries, and injected through wells, trenches or using appropriate tools such as direct push equipment. The design of such a field-scale injection of engineered NP suspensions for the remediation of a polluted site requires a reliable estimation of the particle distribution after injection. In addition, regulators will require information on the long term mobility of the injected particles that may remain in the subsurface after reaction with the contaminant.

In this deliverable, we present modelling tools that are intended to be used in the design of a nanoremediation and in the interpretation of the outcomes. This applies to both preliminary laboratory tests as to field-scale deployment. The development and functionality of the modelling tools is described in some detail, and guidance is given on the use of the tools in practical applications.

The advantages of using modelling in nanoremediation design lay in complementing and thereby reducing otherwise too extensive laboratory testing, in the ability to explore in advance different employment options, in guiding the design and execution of the required monitoring, and in testing assumptions.

Modelling results obtained in support of the large scale experiments at the VEGAS Research Facility for Subsurface Remediation, University of Stuttgart (USTUTT) and for the field test performed at the Balassagyarmat site in Hungary (Golder) are presented as examples.

1 Introduction

1.1 NanoRem WP7: Modelling tool for nanoparticle mobility and interaction with contaminants

The design of a field-scale injection of engineered nanoparticle (NP) suspensions for the remediation of a polluted site requires a reliable estimation of the particle distribution after injection. In addition, regulators will require information on the long term mobility of the injected particles that may remain in the subsurface after reaction with the contaminant.

Numerical models to simulate the transport of dissolved contaminants in aquifer systems are widely available. Several particle transport simulation tools have been proposed and validated to simulate laboratory-scale processes (e.g. column transport tests, represented in 1D geometry). However, well established field-scale NP transport models are not yet available, and the definition of proper approaches and numerical tools, usually based on the up-scaling from simpler geometries and smaller scales, is a current research topic.

In this context, the objectives of the work package of NanoRem that focussed on particle transport modelling (WP7) have been to develop a user-friendly tool for the simulation of NP transport. The tool aims to:

- aid in the design and interpretation of laboratory tests, and
- enable prediction of NP fate and transport and effectiveness at the field scale.

The approach towards the WP7 objectives has been twofold: on the one hand by increasing the understanding of NP behaviour at the pore-scale, and on the other hand on by developing macro-scale tools which can be used to forecast NP behaviour during and after the injection (Figure 1).

1.2 This Deliverable

The theoretical background on NP transport in porous media, the overall approach followed in the development of the pore-scale and macro-scale modelling, and the initial results have been described in NanoRem DL7.1 (Tosco et al., 2016). In this current deliverable we present the final outcomes and tools that have been developed, and the resulting conclusions and recommendations in a comprehensive way. To allow independent reading of the current report, some parts of DL7.1 are reiterated. Chapters 2 and 3 describe the results and tools emerging from the pore-scale (Deltares) and macro-scale (Polito) modelling respectively. Chapter 4 explains how to use NP transport modelling in practical applications. Chapter 5 presents the modelling results obtained by Polito in support of the large scale experiments at the VEGAS Research Facility for Subsurface Remediation, University of Stuttgart (USTUTT) and the field test performed at the Balassagyarmat site in Hungary (Golder). Overall conclusions are summarized in Chapter 6.

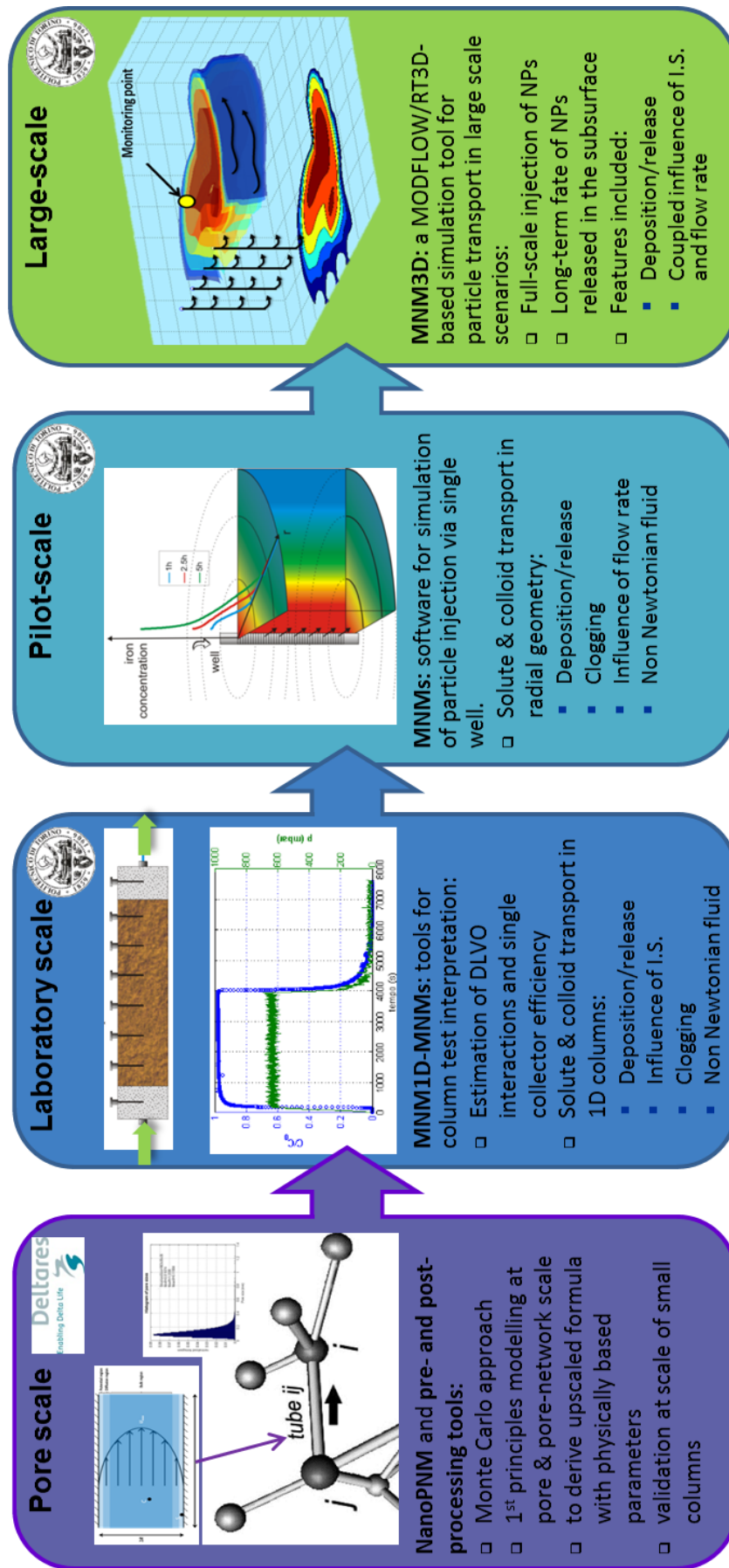


Figure 1: NanoRem WP7 in a nutshell

2 Pore-scale modelling

2.1 Models and tools developed

2.1.1 The NanoPNM model

The existing pore network model of Raouf (Raouf and Hassanizadeh, 2010; Raouf et al., 2010, 2013) was adapted to develop NanoPNM, a numerical code for pore-scale simulation of NP transport. In this model, pores are positioned at a regular grid with lattice distance LD . A lognormal size distribution is defined with mean pore size m and standard deviation s . Each pore can potentially be connected to 26 neighbouring pores (Figure 2), actual connectivity is randomly defined by an elimination rate E ($0.8 \leq E < 0.9$). For a sandy porous medium (PM), LD is in the order of 0.3-0.4 mm, a typical model network of 30 by 30 by 100 nodes then represents a 'column' of 3-4 cm in length and $0.8-1.4 \text{ cm}^2$ in cross-section. Larger networks can be modelled, but computing time increases approximately linearly with the number of nodes as well as linearly with the simulation period.

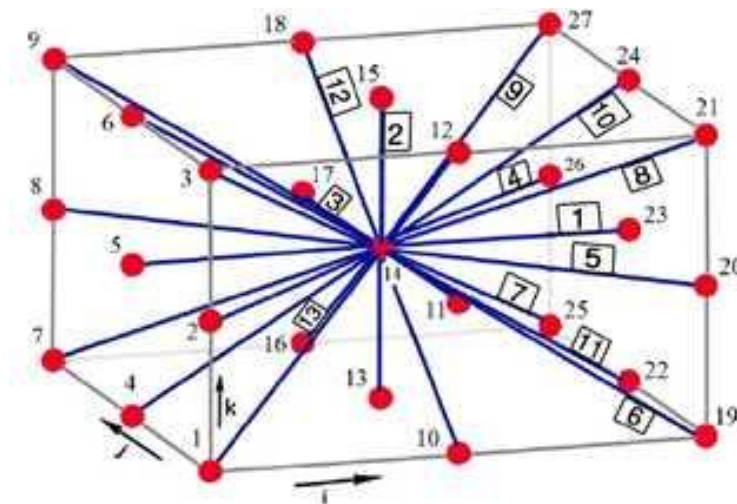


Figure 2: The 26 possible pore throats (pipes) for central pore nr. 14 in 3-dimensions (Raouf and Hassanizadeh, 2010). Numbers in a box represent the direction number 1-13.

The combined set of input parameters LD , m , s , and E define the porosity ϕ and hydraulic conductivity K of the PM represented (Darcy scale) and, in combination with the hydraulic gradient imposed, also the dispersivity α by fitting the simulated breakthrough curve of a (non-adsorbing) tracer. The breakthrough curves are created by running a model with an initial inflow concentration of unity until the outflow concentration equals 0.7 (the pulse time), after which the inflow concentration is set to zero. Then simulation continues until the outflow concentration gets below 0.005.

Additionally, in combination with rules for colloid attachment and detachment at the scale of a single pore, as derived by Seetha et al. (2015), breakthrough curves for NPs at the Darcy scale are simulated, from which attachment and detachment rates at this scale are derived using macro-scale models (see 2.2).

2.1.2 Pre- and post-processing tools for NanoPNM

Because the parameters m , s and E generate random variability, the NanoPNM model is always run several times for a given set of input parameters to obtain a statistical average for the Darcy scale

output parameters. To facilitate the generation of these multiple inputs and the averaging and interpretation of the multiple outputs pre-processing and post-processing tools were developed.

The pre-processing process is summarized in Box 1 and graphically represented in Figure 3. The batch file that is created is read by NanoPNM (Box 2). The post-processing is summarized in Box 3 and graphically represented in Figure 4. Using these tools, outputs (breakthrough curves of tracer and NPs) were generated for a range of pore network characteristics (as defined by the NanoPNM input parameters) and varying PM and NP-slurry characteristics like NP size, flow velocity, PM and NP surface charges, and solution ionic strength.

Box 1: Pre-processing

- a. Open *inputparGenerator.m* and run. Note that *inputparGenerator.m*, *porenetworkGenerator.m*, and *randraw.m* need to be in the same folder
- b. Customize the input files as required.
 - I. Specify a log-file name
 - II. Provide file names and number of files to create
 - III. Decide whether to use identical pore radius distribution or not
 - IV. Decide whether to provide the same statistical setup for pore radius distribution
 - V. Decide the direction of pore throats
 - VI. Choose 'Yes' for the tracer test or 'No' for nanoparticle transport simulation
 - VII. Define minimum, maximum, variance, and mean pore radii
 - VIII. Define the domain size, pore throat elimination rate, lattice distance, ratio of pore radius and pore throat, and inlet/outlet pressure
 - IX. (for nanoparticle transport only: define ionic strength, temperature, particle diameter, zeta potential of the particle and zeta potential of the porous medium)
- c. Input folders, a log file, and a batch file are created

Box 2: NanoPNM

- a. Run the *runNanoPNMsim.bat* file. Note that the batch file created in the pre-processing step, input folders, and NanoPNM.exe are located in the same folder.
- b. Output files, including BTC.txt, are created and stored in the output folder in the files as defined in the pre-processing step.
- c. Units are in **mm** and **min**.

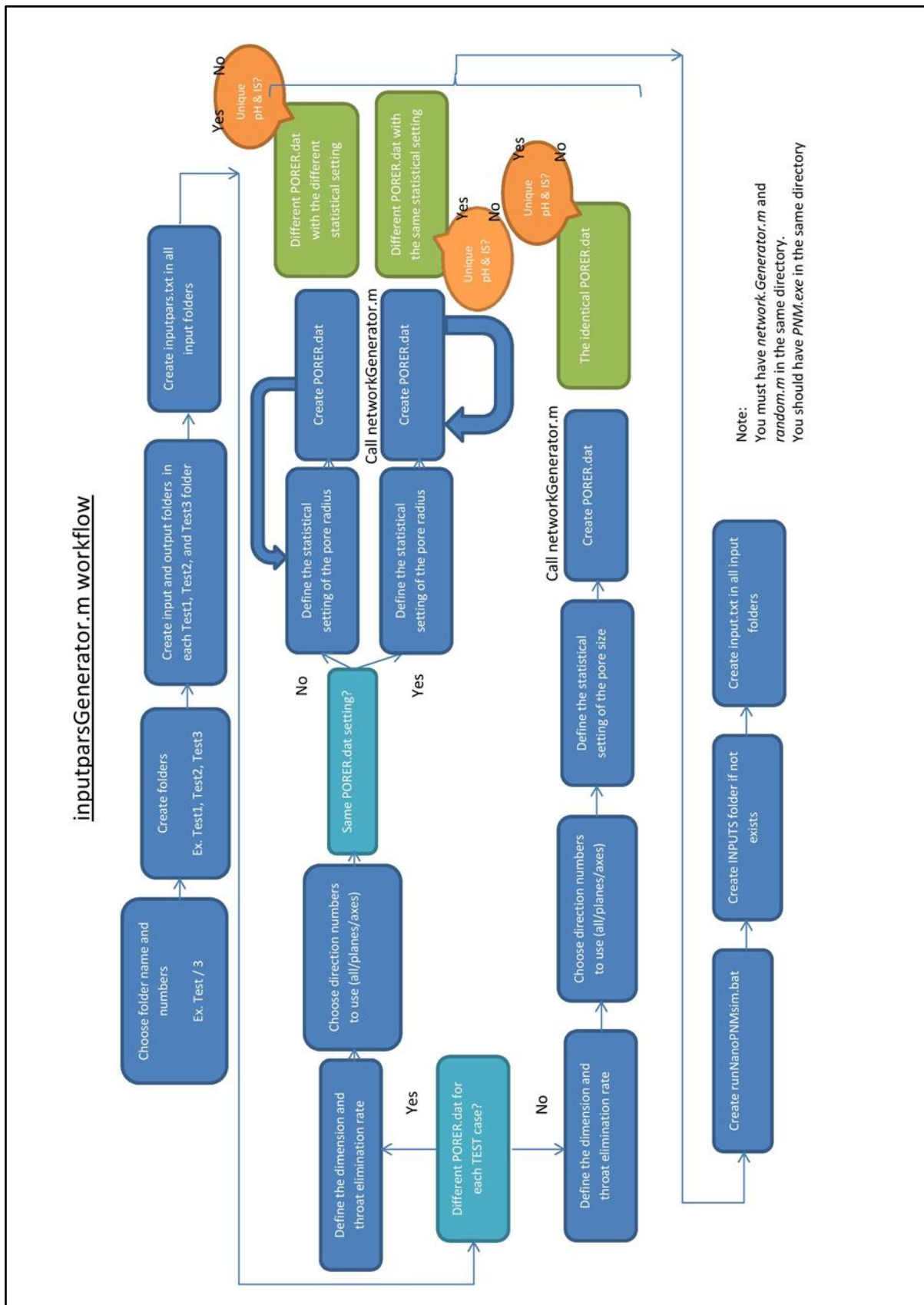


Figure 3: Flowchart of NanoPNM pre-processing

Box 3: Post-processing

- a. Make sure that the following files are in the same folder
 - 1 *BTC.txt* (contains breakthrough data from pore network model),
 - 2 *parm.dat* (contains data of model dimension, Darcy velocity and solute pulse time from pore network model)
 - 3 *input_template.txt* (contains fixed MNMs input data)
 - 4 *param0.dat* (determines which parameters are to be estimated; porosity and dispersivity for tracer test and attachment and detachment rates for nano-particle transport)
 - 5 *MNMs-batch.bat* (batch file running MNMs batch version),
 - 6 *MNMs_NanoRem.exe* (batch version of MNM)
- b. In “*param0.dat*”, the parameters that are to be estimated are defined and an initial guess of these parameter values is given. In the file “*input_template*” fixed model parameters are defined. Parameters from that file, together with specific data from the pore network model in “*parm.dat*” (pulse time, network length, darcy velocity) and the estimation parameters are combined to create the file “*input.txt*” for the Batch version of MNMs. This procedure is part of the optimization code.
- c. Run the *optimizationcode*
- d. The file *paramest.dat* contains the fitted parameters. If the simulation is successful, you see the breakthrough data of the pore network model “*BTC.txt*” and the upscaled model “*output.txt*” are close to each other.

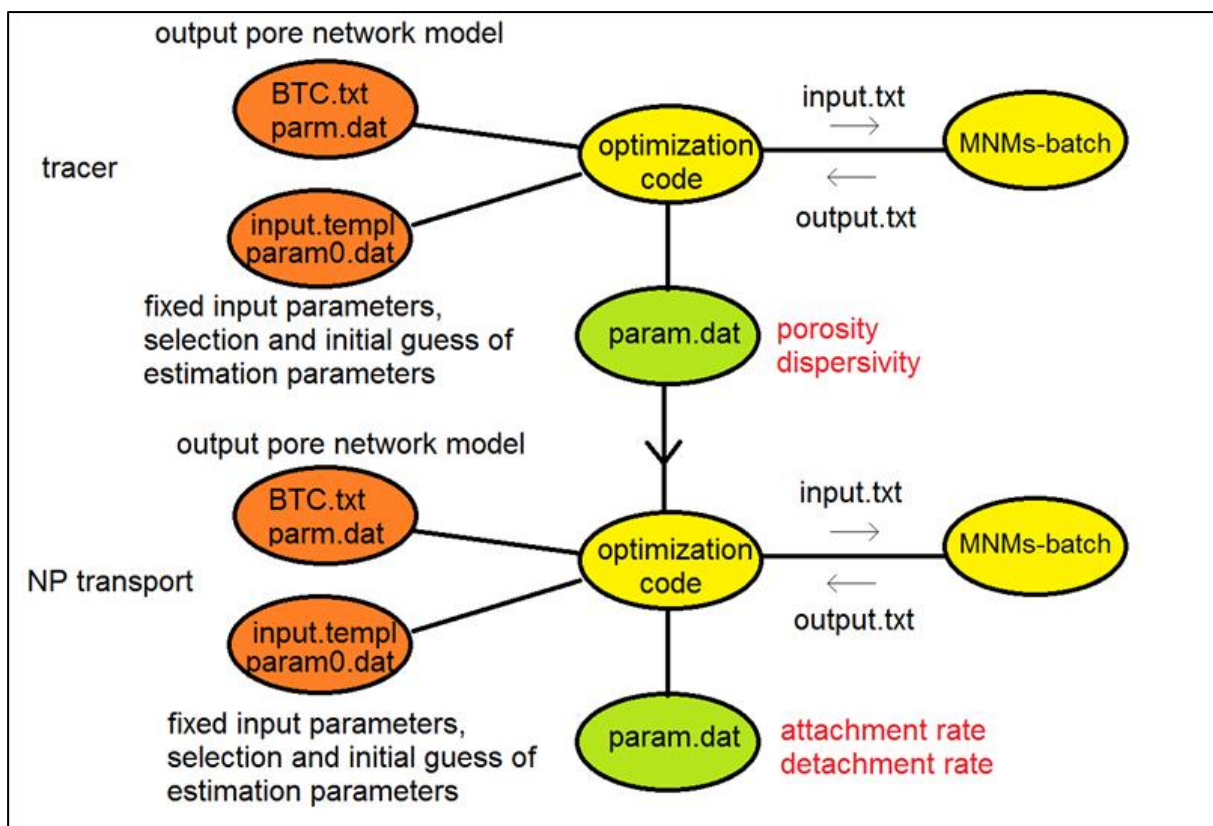


Figure 4: Flowchart of NanoPNM post-processing

2.1.3 Optimization tool for NanoPNM setup

The pore network model is meant to support experiment setups and verifications. In practice, however, the available data that describe a porous medium column usually are grain size distributions, not pore size distributions as needed in NanoPNM. An estimation of the pore size based on the grain size is challenging since heterogeneity or sortedness of grain size and packing influence the pore size distribution.

In the optimization tool, a large number of possible combinations of mean pore radius and standard deviation, lattice distance, and elimination rate are created, which are based on known ranges for porous media from the literature. The resulting NanoPNM porosity, conductivity and dispersivity for each combination are then compared to the experimental data available. To this end, the optimization tool makes use of the upscaled equations developed to calculate these outputs in a fast way (see 2.2 below). The outputs are ranked in order of optimal matching.

2.2 Model results and conclusions drawn

2.2.1 Tracer flow

The formula for tracer flow at the pore scale in NanoPNM are derived from the Poiseuille equation for laminar flow and the Hagen-Poiseuille equation that relates pore discharge/velocity to the pressure gradient, fluid viscosity, and the pore dimensions (length L and radius R). They were used to simulate a large number of very small column tests, from which upscaled rules for hydraulic parameters at the Darcy scale of a porous medium subdomain were derived; the regression equations are shown in Table 1. In the equations for the dispersivity α , the term Nx represents the number of nodes in the flow direction, the length of the modelled domain in the flow direction Lx is equal to $Nx \cdot LD$. It is assumed that LD is a proxy for the median grain size d_{50} .

Table 1: Regression equations for hydraulic parameters

Parameters	Equation	R ²	RMSQE rel.	RMSQE abs.
NanoPNM input parameters	$\phi = 26.0 \left(\frac{m}{LD}\right)^{1.75} \left(e^{s/m}\right)^{-0.55} (1 - E)$	0.998	1.1%	0.0035
	$K = 3.04 \cdot 10^6 \left(\frac{m}{LD}\right)^{2.75} m^2 \left(e^{s/m}\right)^{-2} (1 - E)^{2.25}$	0.997	3.2%	0.84
	$\alpha = 0.243 Nx^{0.1} LD \left(e^{s/m}\right)^{1.55} (1 - E)^{-0.7}$	0.991	1.6%	0.024
porosity and LD	$K = 650 \phi^{2.5} LD^{1.7}$	0.979	8.2%	2.1
	$\alpha = 0.53 Nx^{0.1} \phi^{-0.5} LD^{0.2}$	0.720	9.3%	0.13
porosity, LD, E	$K = 395 \phi^{2.75} LD^{2.1} (1 - E)^{-0.5}$	0.996	3.7%	0.84
	$\alpha = 0.32 Nx^{0.1} \phi^{-0.25} LD^{0.6} (1 - E)^{-0.5}$	0.885	6.0%	0.085

The regression statistics show that porosity and grain size alone are incomplete predictors for hydraulic conductivity and especially dispersivity. The grain packing, in the equations of Table 1 represented by the elimination rate E (inverse of pore connectivity), plays an independent role. This also

implies that hydraulic conductivity and dispersivity from packed columns may differ between different columns as well as from the actual field values. Ideally, laboratory tests should be performed on undisturbed columns, but at least a NP breakthrough test should always be combined with a tracer test for the exact same column.

2.2.2 Nanoparticle breakthrough

For NP attachment and detachment kinetics, we used results from model simulations at the scale of a single pore performed by Seetha et al. (2015), to derive basic rules for NP attachment and detachment at this scale as a function of pore size, flow velocity, NP size and surface charge, surface charge of the porous medium, and physical (temperature, viscosity, dielectric constant) and chemical (ionic strength, pH) properties of the transporting fluid. The dependents are expressed as dimensionless parameters as defined in Table 2. The single-pore equations derived (Table 3) are simplifications of a more extensive set of equations given by Seetha et al. (2015). They show the existence of two main domains, one where surface charge repulsion between NP and PM is limiting NP attachment ($\lambda^* \times N_{E1} \geq 40$, unfavourable conditions), and one where surface charges are much smaller ($\lambda^* \times N_{E1} \leq 15$, favourable conditions). In between, there is a strong and relatively complex dependency on λ^* , N_{E1} and N_{DL} .

Table 2: Parameters used in the equations for attachment and detachment rates at the single pore scale

Dimensional Parameter	Definition	Dimensionless Parameter	Definition
a	NP radius [L]	λ^*	λ / a ($\lambda = 100 \text{ nm}$)
R	Pore radius [L]	A	a/R
v	Pore scale flow velocity [$L T^{-1}$]	Pe	vR/D_∞ ($D_\infty = \frac{k_B T}{6\pi\mu} a$)
IS	Ionic strength [Molar]	N_{DL}	κa ($\kappa = \sqrt{\frac{2000 N_A IS e^2}{\epsilon\epsilon_0 k_B T}}$)
Ψ_{PM}, Ψ_{NP}	Surface potentials on PM, NP [$M L^2 T^{-2} Q$]	N_{E1}	$\frac{\pi\epsilon\epsilon_0}{k_B T} [\Psi_{PM}^2 + \Psi_{NP}^2] a$
$k_{att,pore}$	Pore scale attachment rate [T^{-1}]	Da_{att}	$k_{att,pore} R / v$
$k_{det,pore}$	Pore scale detachment rate [T^{-1}]	Da_{det}	$k_{det,pore} R / v$
$K_{D,pore}$	Pore scale distribution coefficient [L^3/L^2]	$k'D$	$K_{D,pore} / R$
T	Absolute temperature [Θ]		
Physical constants used		Value	
k_B	Boltzmann constant	$1.38 \cdot 10^{-23} \text{ J K}^{-1}$	
μ	Dynamic viscosity	$10^{-3} \text{ kg m}^{-1} \text{ s}^{-1}$ (water at 293 K)	
N_A	Avogadro number	$6.023 \cdot 10^{23}$	
e	Elementary charge	$1.6 \cdot 10^{-19} \text{ C}$	
ϵ	Dielectric constant	80.2 (water at 293 K)	
ϵ_0	Permittivity of vacuum	$8.85419 \cdot 10^{-12} \text{ C}^2 \text{ J}^{-1} \text{ m}^{-1}$	

Table 3: Equations for the rate of attachment and detachment at the scale of (i.e. averaged over) a single pore. For the explanation of the parameters used see Table 2.

Surface potential range	Equations (obeying the relation $k'D = \frac{Da_{att}}{2Da_{det}}$)
$\lambda^* \times NE_1 \geq 40$	$Da_{att} = 0.158 \lambda^{*1.5} e^{-0.5\lambda^*} A^{0.5} e^{-400A} Pe^{-1.1} N_{DL}^{0.5} N_{E1}^{-0.15}$ $Da_{det} = 6.40 \lambda^{*0.5} e^{-0.3\lambda^*} A^{-0.1} e^{-400A} Pe^{-0.9}$ $k'D = 0.0124 \lambda^{*1.0} e^{-0.2\lambda^*} A^{0.6} Pe^{-0.2} N_{DL}^{0.5} N_{E1}^{-0.15}$
$15 < \lambda^* \times NE_1 < 40$	$Da_{att} = 1.78 e^{-1.5\lambda^*} e^{-250A} Pe^{-1.0} e^{0.03N_{DL}} e^{-0.25N_{E1}}$ $Da_{det} = 1.40 \times 10^{-3} e^{0.5\lambda^*} A^{-0.8} e^{-200A} Pe^{-0.9} e^{-0.02N_{DL}} e^{0.03N_{E1}}$ $k'D = 6370 e^{-2\lambda^*} A^{0.8} e^{-50A} Pe^{-0.1} e^{0.05N_{DL}} e^{-0.28N_{E1}}$
$\lambda^* \times NE_1 \leq 15$	$Da_{att} = 0.0872 e^{-1.0\lambda^*} A^{-0.5} e^{-120A} Pe^{-1.0} N_{DL}^{0.1} e^{-0.1N_{E1}}$ $Da_{det} = 2.03 \times 10^{-11} e^{3\lambda^*} A^{-1.3} e^{-120A} Pe^{-1.0} N_{DL}^{-0.4} e^{1.0N_{E1}}$ $k'D = 2.15 \times 10^9 e^{-4\lambda^*} A^{0.8} N_{DL}^{0.5} N_{E1}^{1.1} e^{-1.1N_{E1}}$

Below, results are shown for two typical NanoPNM model runs. The outcomes of the NanoPNM runs were fitted with the macro-scale model MNMs (see Chapter 3.2.1). Input and derived parameters of the pore network model and fitted parameters of the upscaled model are shown in Table 4.

Table 4: Input and derived parameters for pore network model and fitted parameters for upscaled model for two typical examples

parameter	example 1	example 2
length	21.83 mm	21.83 mm
pulse time	70 s	12078 s
min. pore radius	0.018 mm	0.018 mm
max. pore radius	0.42 mm	0.42 mm
average pore radius	0.11 mm	0.11 mm
pore velocity	19.97 mm/min	0.11 mm/min
zeta potential particle	-0.575 mV	-11 mV
zeta potential grain	-1.5 mV	-11 mV
ionic strength	2.3 mM	2.3 mM
particle diameter	1000 nm	200 nm
NE_1	1.41	13.2
N_{DL}	157	15.7
λ^*	0.2	1
A	0.00238 - 0.056	0.00048 - 0.011
average attachment rate	$4.23 \cdot 10^{-5} \text{ s}^{-1}$	$1.10 \cdot 10^{-4} \text{ s}^{-1}$
average detachment rate	$2.91 \cdot 10^{-13} \text{ s}^{-1}$	$1.36 \cdot 10^{-4} \text{ s}^{-1}$
fitted porosity	0.373	0.374
fitted dispersivity	1.18 mm	1.20 mm
fitted attachment rate	$8.05 \cdot 10^{-5} \text{ s}^{-1}$	$3.46 \cdot 10^{-5} \text{ s}^{-1}$
fitted detachment rate	$8.94 \cdot 10^{-8} \text{ s}^{-1}$	$7.38 \cdot 10^{-5} \text{ s}^{-1}$

In the first example, the adsorption of NPs is limited and the breakthrough curves resemble that of the tracer (Figure 5). The NP breakthrough curve as simulated by NanoPNM is only marginally different from the tracer breakthrough curve. The MNMs macro-scale fit for the NP shows a better fit in comparison to the fit for the tracer. That is due to the fact that there are more adaptable fitting parameters: by updating the adsorption and desorption rates, in addition to porosity and dispersivity, it gives the model the opportunity to reduce the misfit further.

In this case, the estimated macro-scale attachment and detachment rates have much larger values than the attachment and detachment rates of the individual pore throats in the pore network model. The obtained attachment and detachment rates here are due to an additional upscaling of the physical properties (distribution of pore and pore throat radii and pore connectivity) of the porous medium.

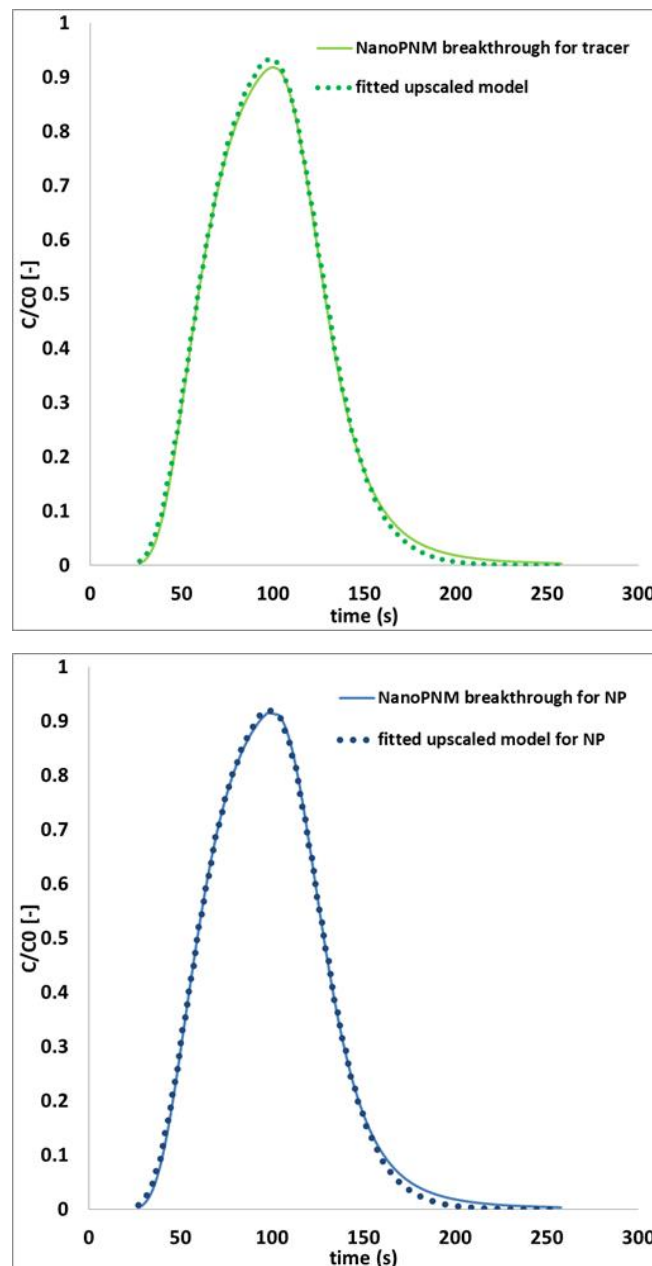


Figure 5: Breakthrough curve data from the pore network model and the fitted upscaled model for a tracer (green, top) and a hypothetical NP (blue, bottom) for a situation with limited adsorption of NP (example 1 of Table 4)

The second example shows a situation with significant adsorption and the breakthrough of the NP is retarded and is more skewed compared to the breakthrough of the tracer as shown in Figure 6. For this model the individual pore scale attachment and detachment rates and their effective upscaled rates are shown in Figure 7. The upscaled values of the adsorption and desorption rate are in the lower range of values in the individual pore throats of NanoPNM, suggesting that the average values would not provide a good estimate for the upscaled values.

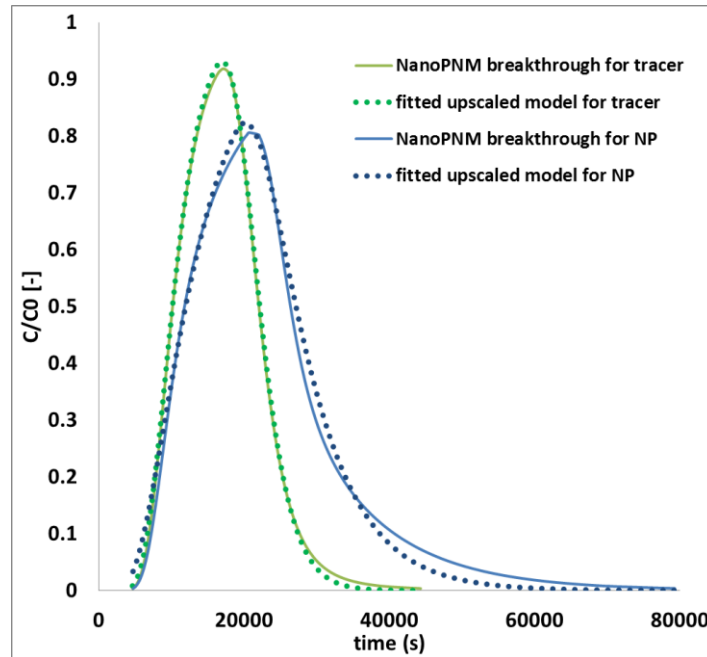


Figure 6: Breakthrough curve data from the pore network model and the fitted upscaled model for a tracer (green) and a hypothetical NP model (blue) for a situation with strong adsorption of NP (example 2 of Table 4)

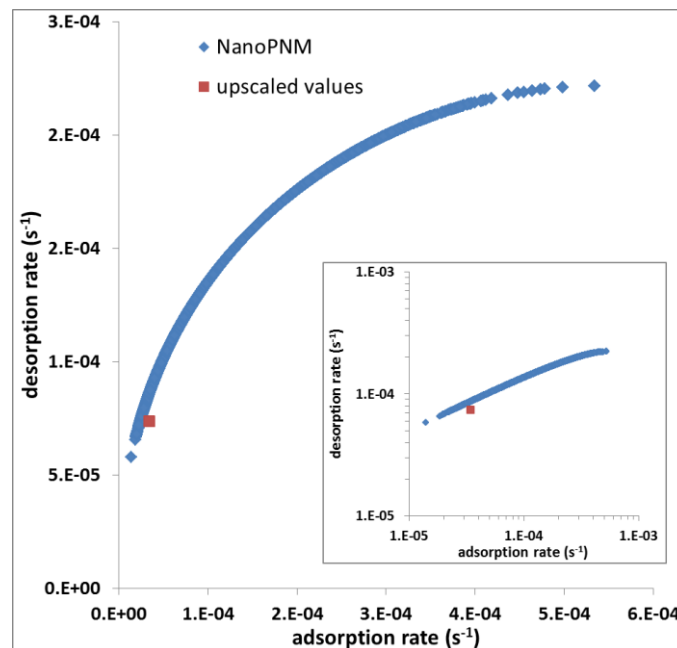


Figure 7: Attachment and detachment rates for the individual pore throats in the NanoPNM pore network model and the effective values of the fitted upscaled model for example 2 of Table 4. The inset shows the same data using logarithmic axis-scales.

Figure 8 shows the histogram of both the attachment and detachment rate of the pore throats in the pore scale model. The values of the upscaled model (attachment rate = $3.46 \cdot 10^{-5} \text{ s}^{-1}$; detachment rates = $7.38 \cdot 10^{-5} \text{ s}^{-1}$) are also smaller than the median of the distribution of the pore network model. This confirms that local scale conditions in the tail of the overall distribution of conditions can dominate upscaled behaviour.

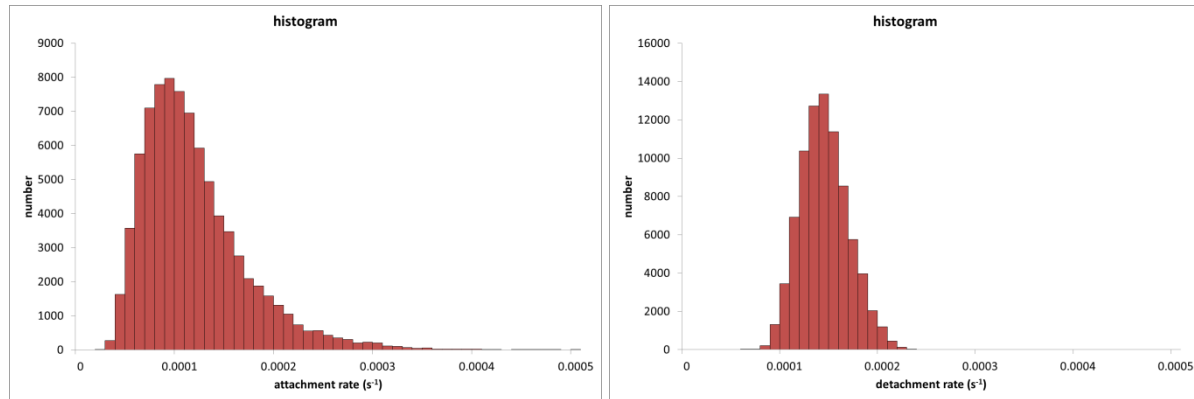


Figure 8: Histograms of attachment rates (left) and detachment rates (right) in the pore network model

In order to check the applicability of derived parameter relationships, it would be desirable to compare predicted model results based on the upscaling relationships with laboratory experiments as performed in e.g. WP4. However, reported parameters indicate that basically all experiments would fall into the domain of unfavourable conditions. The surface charge of sandy PM is predominantly negative, according to literature the zeta potential for quartz sand varies roughly between -15 mV and -40 mV, depending on pH and salt content of the pore liquid (Redman et al., 2004; Júnior & Baldo, 2014). The NPs investigated within NanoRem are engineered to also obtain a –preferably strongly– negative zeta potential, to aid both in the stabilization of the NP slurry as in NP transport within an aquifer. Their zeta potentials are reported to vary between -20 mV and -60 mV (Micic Batka et al., 2016). For such conditions, the fundamental modelling analysis by Seetha et al. (2014, 2015) - and hence NanoPNM when using the equations of Table 3 - does not predict any NP attachment.

Significant retention of NPs only seems possible for much lower zeta potentials. It was therefore hypothesised that both NP and PM are not sufficiently characterized by just their average zeta potential, and that the domain averaged NP behaviour might be dominated by the occurrence of less negative (or even partly positive) surface sites. A similar suggestion was made to explain observed differences in NP breakthrough in columns with either Dorsilit® sand (M.I) or VEGAS sand (M.II) (Hofmann et al., IDL 4.2).

We therefore investigated to what extent observed NP breakthrough curves, especially their dependence on ionic strength, could be explained by using “effective” surface charges. We used the experiment of Carbo-Iron® as reported in Micic Batka et al. (2015) and fitted the breakthrough curve of the soft (water type F.I.s) and hard (water type F.I.h) water experiments with MNMs. We compared the resulting ratio between the fitted macro-scale rates for the two water types (both attachment and detachment rate) with the ratio obtained when using the equations of Table 3 in NanoPNM using the reported ionic strengths for F.I.S and F.I.h.

Figure 9 shows the experimental and the macro-scale modelled breakthrough of the Carbo-Iron[®] experiments for the water types F.I.s and F.I.h. Table 5 lists the fitted macro-scale attachment and detachment rates for the two water types and their ratio, together with the ratio calculated using the equations given in Table 3 for the condition $\lambda^* \times NE1 \leq 15$. For the detachment rate, the ratio of the values for the two water types based on the pore scale equations gives a good match with the ratio obtained in the laboratory experiment, but for the attachment rate the effect of the ionic strength is underestimated in the pore network equations.

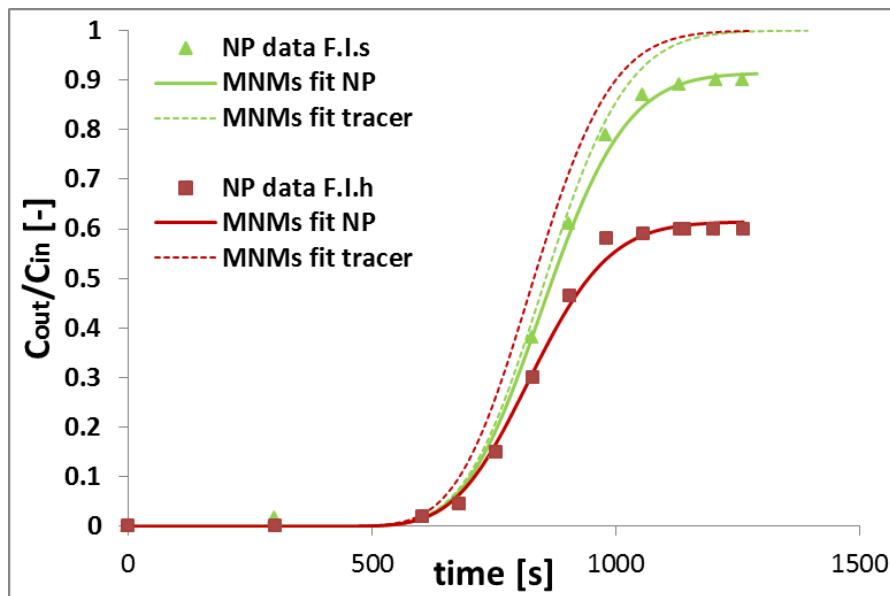


Figure 9: Experimental and macro scale modelled breakthrough curves for the Carbo-Iron[®] column experiment; left using water type F.I.s; right using water type F.I.h

Table 5: Comparison of the ratio of the parameters for the two water types for both fitted experimental data and the upscaling equations

	Lab experiment			Pore scale equations
	F.I.s	F.I.h	ratio	ratio
attachment rate	1.07E-04 (s ⁻¹)	5.94E-04 (s ⁻¹)	0.18	0.90
detachment rate	2.95E-05 (s ⁻¹)	2.04E-05 (s ⁻¹)	1.44	1.52

2.2.3 Conclusions on NP transport

A pore-network model has been developed based on a pore-scale description of major processes affecting the fate of particles. The model can be used to relate macro-scale sorption parameters to the underlying pore-scale variables such as solution pH and ionic strength, zeta potential of nanoparticles and grains, nanoparticle sizes, pore sizes, and water flow velocity. In this regard, relationships for pore-scale attachment and detachment as functions of these variables are needed. Those relationships were obtained by solving particle transport equations in a cylindrical pore with smooth surfaces and uniform surface properties. However, using those relationships, our pore-scale model showed less attachment of nano-particles than observations. We observed that, for the average or median conditions of NP and porous media surface charges, no significant NP attachment is predict-

ed. Significant retention of NPs is only possible for much lower zeta potentials, which might be the “effective” surface charges in the tail of the surface charge distributions that dominate the upscaled behaviour. However, at the flow velocities that occur during NP slurry injection, calculated attachment rates are low compared to advective transport, and NP attachment is only predicted for relatively long residence times. This does not seem to agree with observations from laboratory columns, where NP attachment is observed to occur already close to the inlet. Furthermore, while the observed dependency of the detachment rate on ionic strength might agree with the theory-based predictions, for the attachment rate the effect of the ionic strength is clearly underestimated in the pore network equations. Therefore, we conclude that the commonly used variables (solutions pH and ionic strength, zeta potential of nanoparticles and grains, nanoparticle sizes, pore sizes, and water flow velocity) are not enough to effectively predict colloid retention under environmental conditions. Other possible factors including grain surface roughness, surface chemical heterogeneity, and particle-particle interaction can contribute to the enhanced NP adsorption. The evaluation of these factors should be explored using microscopic and columns scale experiments under controlled conditions.

3 Macro-scale modelling

3.1 Mechanisms controlling particle transport in porous media

When NPs are dispersed and transported within groundwater, they are subject to processes like filtration, straining, physical-chemical deposition and aggregation, as they are attracted to the surfaces of the PM grains and to each other (Figure 10). The dynamic processes of attachment and detachment of NPs are governed by physical laws that operate at the scale of grains and pores, but impact the transport behaviour of NPs at the macro (Darcy) scale (Crevacore et al., 2016).

At the macro-scale - i.e. the scale of interest for field applications of NP-based remediation -, NP transport in porous media is usually described by a modified advection-dispersion equation that takes into account the mass exchanges between liquid and solid phase due to physical and physico-chemical interactions:

$$\phi \frac{\partial c}{\partial t} + \sum_i \rho_b \frac{\partial s_i}{\partial t} + q \frac{\partial c}{\partial x} - \phi D \frac{\partial^2 c}{\partial x^2} = 0 \quad (\text{eq. 1})$$

$$\rho_b \frac{\partial s_i}{\partial t} = \phi k_{att,i} f_{att,i} c - \rho_b k_{det,i} s_i \quad (\text{eq. 2})$$

where c is the NP concentration in the liquid phase [L^{-3}], s is the NP concentration in the solid phase [M^{-1}], ϕ is porosity [-], ρ_b bulk density of the PM solid matrix [$M L^{-3}$], q is the Darcy velocity [$L T^{-1}$], D is the dispersion coefficient [$L^2 T^{-1}$], k_{att} , k_{det} are the NP attachment and detachment rate coefficients [T^{-1}], f_{att} are functions [-] depending on the process(es) being described (Figure 10). The subscript i refers to the i -th retention mechanism: NP retention may be due to more than one mechanism, for example due to heterogeneities in the porous medium, or to different concurrent phenomena (e.g. straining due to the presence of large particles, and blocking due to particle-particle interactions). An additive effect of concurrent phenomena is usually assumed, $\rho_b \frac{\partial s}{\partial t} = \sum \rho_b \frac{\partial s_i}{\partial t}$. Usually, a maximum of two concurrent phenomena is adopted ($i = 1, 2$).

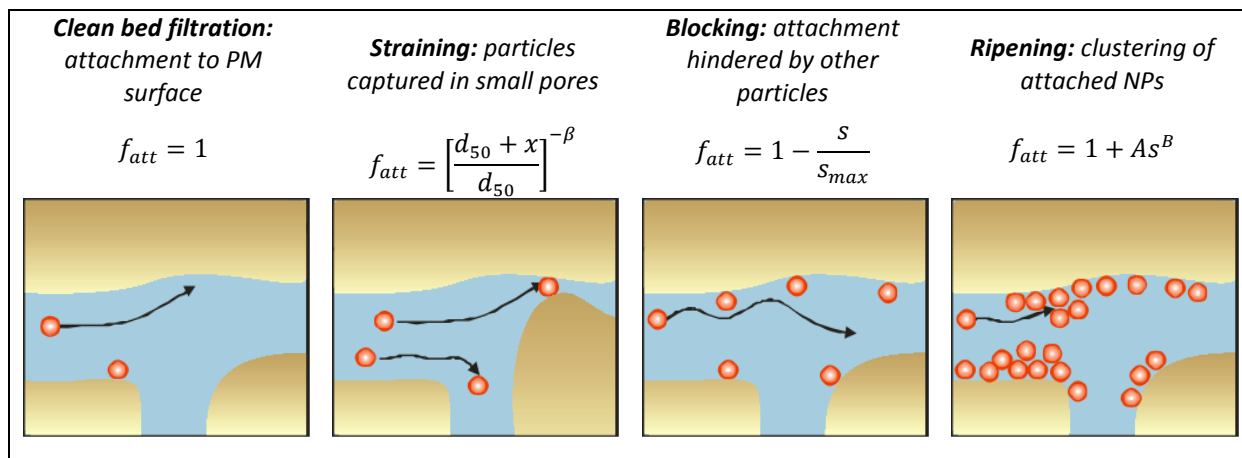


Figure 10: Pore scale particle retention processes; d_{50} is median grain size of the PM; x is distance travelled in the PM domain from the inlet point; β , A , B are fitting parameters. Modified from Tosco et al. (2014b).

As also shown in the previous Chapter 2.2, the type of interaction mechanisms and the magnitude of attachment and detachment kinetics are strongly influenced by factors that depend on both opera-

tive and natural conditions. A NP transport simulation tool effective in assisting the design of a field-scale application of NPs has to take into account these effects in a quantitative, and coupled, way (Tosco et al. 2014a). The following three parameters are of particular importance:

- *flow velocity*: during particle injection e.g. through a well screen, flow velocity decreases hyperbolically with increasing distance from the injection point. The current version of MNMs implements the formulation of k_{att} and k_{det} as a function of pore water velocity v as proposed by Tosco et al. (2014a), based on the single collector removal efficiency (Yao et al. 1971):

$$k_{att}(v) = \frac{3}{2} \frac{(1-\phi)}{\phi d_{50}} p_{att} \eta_0 v \quad (\text{eq. 3})$$

$$k_{det}(v) = p_{det} \mu v \quad (\text{eq. 4})$$

where ϕ is porosity, d_{50} is the average grain size of the porous medium p_{att} [-] and p_{det} [T M^{-1}] are parameters to be determined from fitting of experimental data, μ [$\text{M L}^{-1} \text{T}^{-1}$] is the fluid viscosity, and η_0 [-] is the single collector efficiency, which can be calculated using different correlations, e.g. those proposed by Yao et al. (1971), Rajagopalan and Tien (1976), Tufenkji and Elimelech (2004), Messina et al. (2015).

- *ionic strength*: ionic strength (IS) significantly affects the particle-particle and particle-porous medium interactions. As a consequence, on a longer time frame possible changes in the groundwater salt content may lead to immobilization or re-mobilization of the particles, thus affecting their long term behaviour. In MNMs the semi-empirical constitutive equations proposed by Tosco et al. (2009) are currently implemented:

$$k_{att}(C_{salt}) = \frac{k_{att\infty}}{1 + \left(\frac{CDC}{C_{salt}}\right)^{\beta_{att}}} \quad (\text{eq. 5})$$

$$k_{det}(C_{salt}) = \frac{k_{det0}}{1 + \left(\frac{C_{salt}}{CRC}\right)^{\beta_{det}}} \quad (\text{eq. 6})$$

$$s_{i,max}(C_{salt}) = \gamma_s C_{salt}^{\beta_s} \quad (\text{eq. 7})$$

where the terms k_{att} , CDC , β_{att} , k_{det0} , CRC , β_{det} , γ_s , and β_s are empirical coefficients determined via fitting procedures; C_{salt} is the salt concentration in pore water.

- *fluid viscosity*: NPs suspended in water are in most cases not stable and need to be stabilised by addition of polymers in order to be injected into groundwater. The polymers commonly used in field applications (e.g. guar gum, xanthan gum, CMC, etc.) are characterized by a non-Newtonian rheological behaviour (shear thinning - viscosity changes with changing flow velocity) which influences the overall injection of the suspension. It is known that particle colloidal stability - and consequently mobility in the porous medium - is significantly affected by the viscosity of the carrier fluid. Moreover, the viscosity of the injected fluid also affects the fluid pressure in the aquifer system during injection.

Additionally, clogging, due to the accumulation of significant amounts of particles in the pores of the aquifer, is simulated through the reduction of permeability and porosity induced by deposited particles. In the approach proposed by Tosco and Sethi (2010), the pressure build-up arising from the particle deposition is calculated using a modified formulation of the Darcy's law (Tosco et al. 2014a), which takes into account both the reduction in porosity, permeability, and the possible non-Newtonian nature of the fluid.

3.2 Models and functionality developed

3.2.1 MNMs for 1D modelling of NP transport

MNMs stands for **Micro- and Nano-particles transport, filtration and clogging Model Suite**. It is a complete tool for the simulation of particle transport in 1D saturated porous media and for the interpretation of laboratory column transport test. MNMs represents the evolution of MNM1D (Tosco and Sethi 2009, Tosco et al. 2009) and E-MNM1D (Tosco and Sethi 2010), whose features are integrated here and extended in a user-friendly Matlab-based graphical interface. The structure and main features of the last release of MNMs are provided in Figure 11. A comparison with other existing simulation tools for particle transport is reported in Table 6. MNMs is compiled as a standalone executable file and can be downloaded from the web page of the Groundwater Engineering research group of Politecnico di Torino (<http://areweb.polito.it/ricerca/groundwater/software/MNMs.php>). The reader can refer to the manual of MNMs for a detailed description of tools and equations (<http://areweb.polito.it/ricerca/groundwater/software/MNM1D.html>).

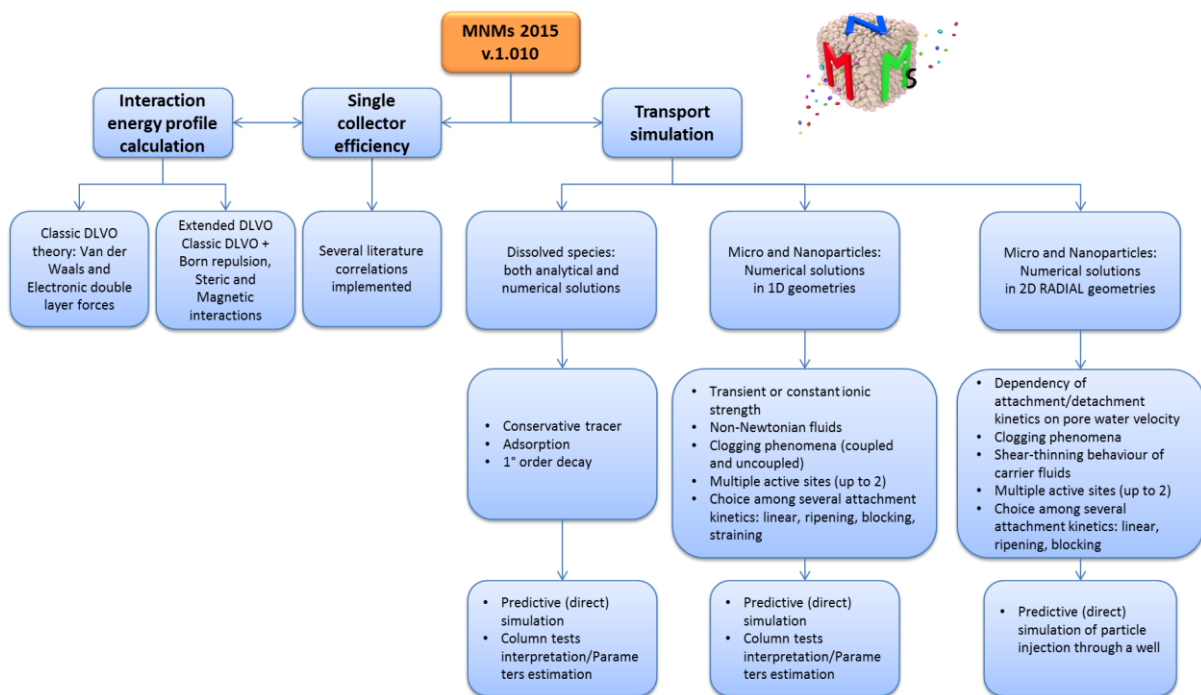


Figure 11: Structure and main features of MNMs

Like many transport simulation models, MNMs can be run in two modes (Figure 12):

- predictive or forward mode: assuming that transport-controlling mechanisms and transport parameters (attachment/detachment and clogging) are known, the model is run once to forecast particle transport;
- inverse mode: assuming transport-controlling mechanisms, and determining the transport parameters (for eg. k_{att} and k_{det}) by fitting the simulation results to experimental data (e.g. breakthrough curves and concentration profiles).

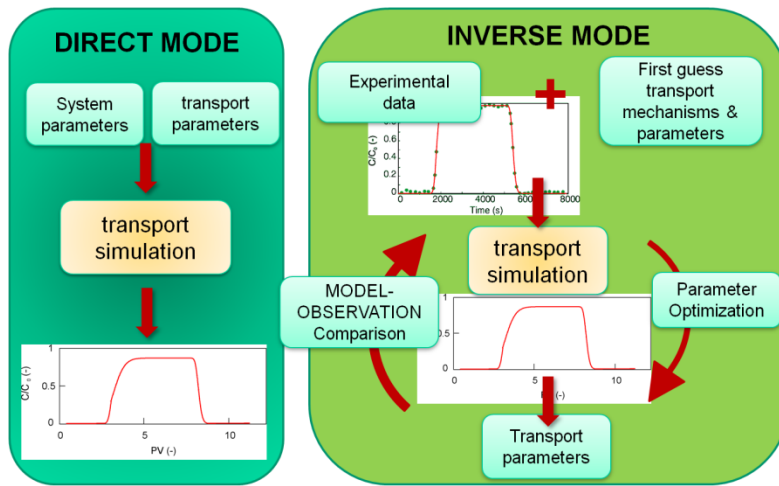


Figure 12: Transport model run in predictive or inverse mode

Table 6: Software comparison: Stanmod, Hydrus-1D and MNMs

		Stanmod	Hydrus-1D	MNMs
Interaction	Single-site	✓	✓	✓
	Multiple-sites	✓	✓	✓
Processes	Classical filtration theory	✗	✓	✓
	Reversible linear attachment	✓	✓	✓
	Blocking	✗	✓	✓
	Ripening	✗	✓	✓
	Straining	✗	✓	✓
	Ionic strength dependency	✗	✗	✓
	Pore-water velocity dependency	✗	✗	✓
Features	Inverse simulation (parameters estimation)	✓	✓	✓
	Extended-DLVO interaction profiles calculation	✗	✗	✓
	Tool for calculation of single collector efficiency	✗	✗	✓
	Flow-transport coupling (clogging)	✗	✗	✓
	Non-Newtonian behaviour of the carrier fluid	✗	✗	✓
	Radial simulation of particle injection	✗	✗	✓

3.2.2 Functionality of MNMs

The main features included in MNMs are:

- **Interaction energy profiles** calculation (Figure 13a) which can be used to estimate particle-particle and particle-collector interaction energy profiles using the DLVO (Derjaguin and Landau, Verwey and Overbeek) and Extended-DLVO (accounting for Born repulsion, steric and magnetic interactions) theory approach. It is useful to forecast the micro- and nano-particle behaviour in terms of aggregation and mobility.
- Calculation of single collector attachment efficiency η_o (Figure 7b): the single collector attachment efficiency is one of the most important parameters for the assessment of the mobility of

micro- and NPs in porous media. MNMs implements a dedicated tool to easily compute η_0 using up to 7 different formulations. Among these, MNMs also implements the novel total flux normalized correlation equation for predicting single-collector efficiency under a broad range of parameters (Messina et al., 2015; Messina et al., 2016) that was developed at Politecnico di Torino.

- Simulation of the **transport of a dissolved species** accounting for equilibrium sorption and first order degradation, useful for simulation of contaminant transport and interpretation of column tracer tests.
- Simulation of **particle transport under transient ionic strength conditions**: MNMs numerically solves the colloidal transport equations taking into account the colloids deposition and release during transients of the carrier fluid (water) ionic strength. Four different types of attachment kinetics can be simulated: linear, Langmuirian with blocking, ripening and straining.
- Simulation of **porous medium clogging phenomena**, when the modification of the column porosity and permeability due to deposition of colloidal particles strongly influences the flow field and cannot be neglected. In this case, MNMs takes into account the variation of pressure drop along the column due to the medium clogging and solves the differential system coupling flow and transport equations.
- Simulation of **particle transport in the presence of Non-Newtonian carrier fluids**: nanoparticles suspended in water are generally not stable and need to be stabilized by addition of polymers in order to be injected in groundwater. The polymers commonly used in field applications (e.g. guar gum, xanthan gum, CMC, etc.) are characterized by a non-Newtonian rheological behaviour (shear thinning) which influences the overall injection of the suspension. MNMs can be used for the interpretation of column transport test where the influence of the suspension rheology cannot be neglected. A generalized Darcy law is used to estimate the pressure build-up due to the non-Newtonian nature of the injected fluid, which is a critical issue for field injections.
- Simulation of **pilot-scale injection of micro- and nanoparticle slurries through a single well** (radial simulation tool). In field applications fluids are typically injected into the subsurface via wells or direct push systems, generating a radial or radial-like flow, with decreasing velocity with increasing distance from the delivery point (Tosco et al. 2014a). Therefore, MNMs solves the system of partial differential equations describing transport of injected particles in a homogeneous infinite porous medium assuming a 1D geometry with radial symmetry (Figure 14). The radial tool takes into account the influence of flow velocity (and then of the injection flow rate) on the kinetics of the particle-porous medium interactions (deposition and release processes), the eventual clogging, and the non-Newtonian (shear thinning) rheological properties of the carrier fluid used to improve the colloidal stability of the suspensions. The empirical relationships proposed in Tosco et al. (2014a) have been used to express the dependence of the deposition and release parameters on the flow velocity. A modified formulation of the Cross rheological model has been implemented to account for the shear thinning behaviour of polymeric stabilizers usually employed for particle injection.

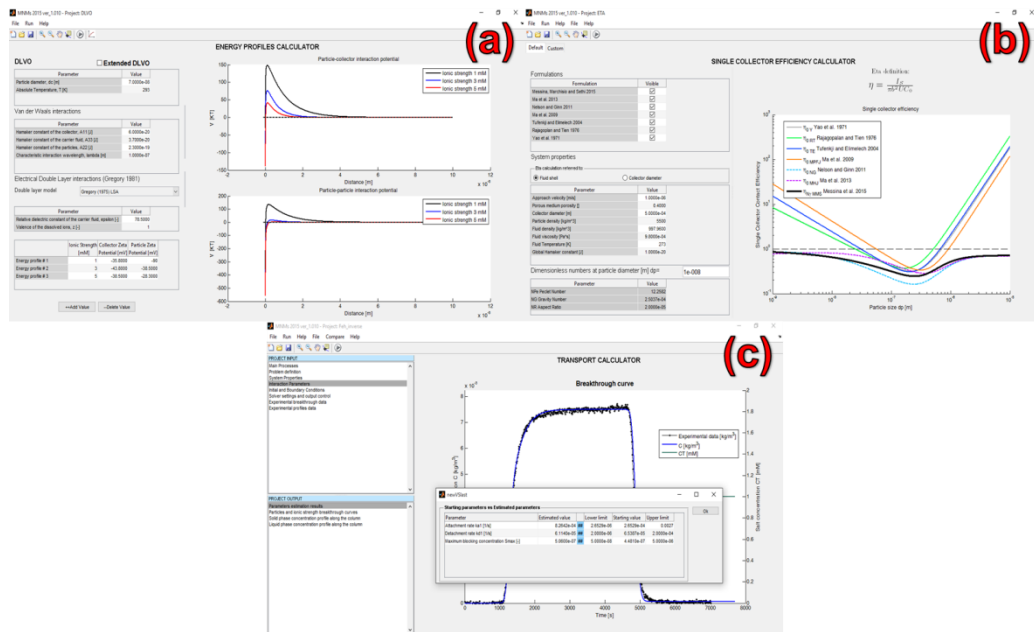


Figure 13: The MNMs graphical interface: (a) DLVO interaction profile calculation; (b) single collector efficiency calculation; (c) particle transport simulation under transient ionic strength conditions.

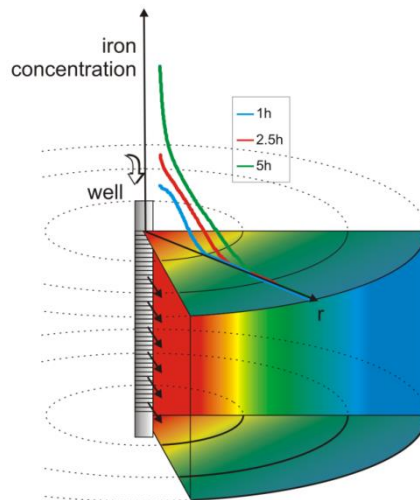


Figure 14: Radial geometry: conceptual model and example of simulation results [modified from Tosco et al. (2014a)].

3.2.3 MNM3D for 3D NP transport modelling

MNM3D, standing for **M**icro- and **N**ano-particles transport **M**odel in **3D** geometries, is a modified version of the transport model RT3D (Clement 1997), in which the NP transport equations are solved in 3D (Bianco et al. 2016). MNM3D solves the NP transport equations 1-2, accounting for dependency of the attachment and detachment kinetics on the groundwater ionic strength (eq. 5-6-7) and velocity (eq. 3-4). In addition, MNM3D implements a new formulation of the attachment and detachment coefficients for the simulation of the simultaneous effects of pore water velocity and ionic strength

(Bianco et al. 2016). To this purpose, the dependency of the empirical parameters $C_{a,i}$ and $C_{d,i}$ on the ionic strength has been explicitly expressed by coupling eq. 3-4 with eq. 5-6:

$$k_{att,i}(v, c_t) = \frac{3(1-\epsilon)}{2 \epsilon d_s} \frac{C'_{a,i}}{1 + \left(\frac{C_{DCi}}{c_t}\right)^{\beta_{a,i}}} \eta_0 v \quad (\text{eq. 8})$$

$$k_{det,i}(v, c_t) = \frac{C'_{d,i}}{1 + \left(\frac{c_t}{C_{RCi}}\right)^{\beta_{d,i}}} \mu v \quad (\text{eq. 9})$$

where $C'_{a,i}$ [-] and $C'_{d,i}$ [T M⁻¹] are fitting parameters which embed all the other phenomena not explicitly considered here.

The particle concentration is solved in space and time for both particles suspended in the liquid phase and attached to the porous medium. Heterogeneities in the hydrodynamic properties of the porous medium and of the particle-soil interactions can be taken into account by implementing space-variable hydrodynamic, transport and kinetic parameters. MNM3D is composed of four different packages that can be alternatively selected according to the phenomena that must be introduced into the simulation: particle transport with reversible linear or non-linear attachment kinetics, ionic strength-dependent transport, velocity-dependent transport, coupled ionic-strength and velocity dependent transport.

MNM3D can be applied both for the short term evaluation of particles distribution around one or more injection points, and for the long term particle spreading prediction. It overcomes many limitations and approximations of the other simplified numerical codes and offers the opportunity to fill the gap between the controlled conditions of laboratory tests and the more complex scenarios typical of field-scale applications. If coupled with MNMs, MNM3D can be used at the final stage of the remediation design process, as a support to estimate important operative parameters, including particles distribution around the injection well, influence radius for a target concentration, number of required injection wells, etc.

MNM3D can be easily implemented in many open-source and commercial graphical interfaces which already support RT3D. MNM3D is currently being implemented in Visual Modflow (Waterloo Hydrogeologic) and will be included as a transport simulation package in the next release of the software in 2017.

3.3 Model validation

In order to validate MNM3D, simulations of particle transport have been performed and compared with experimental data and breakthrough curves simulated by MNMs.

The ionic strength dependent transport kinetics implemented in MNM3D (eq. 1, 6-7, 8) were validated against the experimental data of ferrihydrite nanoparticle transport in saturated sand columns (Tosco et al. 2012). Column tests were performed under transient IS, including injection of ferrihydrite colloidal dispersions at constant IS, followed by flushing with particle-free electrolyte solutions at lower ionic strength to promote the release of reversibly deposited particles.

An example of the validation results is reported in Figure 15. The experimental data were least-squares fitted using MNMs assuming dual-site (linear and blocking), reversible deposition (eq. 1-2-3). The fitted parameters were then used in MNM3D to simulate the same test in direct mode. MNM3D-

simulated breakthrough curves reproduced the experimental data and the MNMs model curve well, with a R^2 value of 0.998 (Figure 15). The two models adequately captured the release peaks which followed the injection of DI water in terms of timing, shape and magnitude. The good overlap of the simulation results of MNMs and MNM3D proved the correct implementation of the ionic strength dependent model into the RT3D user-defined reaction module. The numerical codes were also compared in a wide range of column sizes, injection flow rates, IS and kinetic coefficients values, always providing comparable results (data not reported).

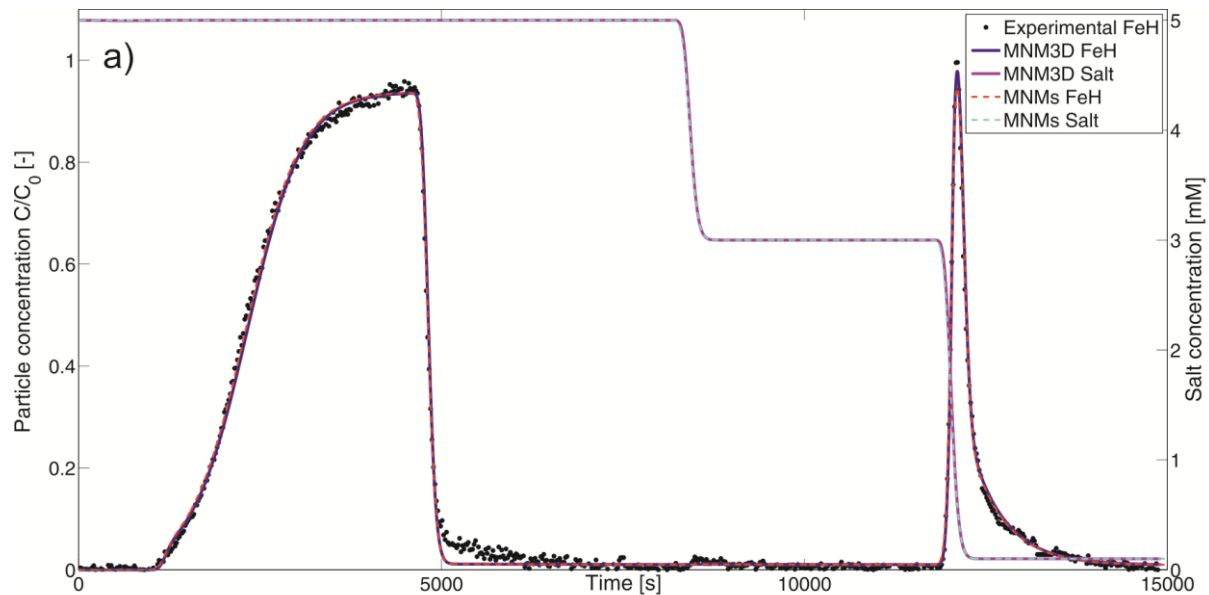


Figure 15: MNM3D validation versus experimental data (dots) and MNMs simulation results. Interpretation of a column test of ferrihydrite nanoparticle (blue solid line for MNM3D and red dashed line for MNMs) transport under transient ionic strength conditions. Ionic strength (purple solid line for MNM3D and cyan dashed line for MNMs) varies from 5mM during the particle injection to 0.1 mM during flushing with freshwater. Experimental data from Tosco et al. (2012).

Simulations of velocity-dependent transport in a radial-symmetric configuration were performed in MNM3D and validated against the results provided under the same scenario by the radial transport module available in MNMs. The model reproduced the radial injection of nanoparticles in a homogeneous porous medium. The injection was carried out through a well having a 25 cm diameter (typical size of wells used for zero-valent iron injection) and screened along the whole aquifer depth. One active site was assumed, with linear reversible attachment kinetics.

Three simulations were performed for three values of particle size in the range of typical size of commercially available NZVI, namely 1.2 μm , 800 nm, 80 nm. The simulation results for MNM3D and MNMs were compared in terms of profile of total concentration, expressed as the sum of the colloid concentration suspended in liquid phase and deposited on the solid matrix (Figure 16b). Very good agreement was observed between the two software output for all particle sizes, with R^2 values always greater than 0.999. Despite the considerable difference in the number (70 of MNM3D against 200 of MNMs) and size of cells along the radial direction that were imposed in the two models, MNM3D showed to be able to reproduce with good accuracy the velocity-dependent kinetics implemented in MNMs. However, a higher computational time was required by MNM3D to calculate the concentration distribution over the full 3D domain.

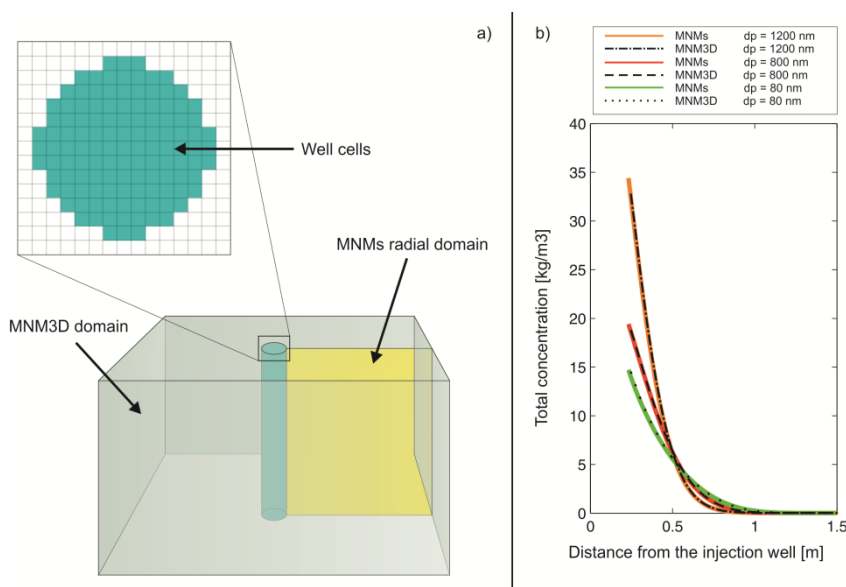


Figure 16: a) Conceptual model of the simulation domains used in MNMs (2D radial) and MNM3D (full 3D). b) MNM3D validation against MNMs simulation results. Injection of micro- and nanoparticles (particle diameter of 1200 nm, 800 nm and 80 nm) through a well having a diameter of 25 cm.

3.4 Discussion and conclusions

The graphical interface MNMs was developed as a comprehensive tool for the simulation of the micro- and nanoparticle transport at laboratory and pilot scale. This software is intended as a complete tool that can provide useful help during all the steps of the design of nanoparticle based remediation, from the particle characterization to the injection design. The calculation of the DLVO interaction profiles and of the single collector efficiency is very useful to quickly assess the expected mobility and stability of particles in the porous medium and design the laboratory column transport tests. The interpretation of breakthrough curves from column tests represents a key aspect to understand the mechanisms governing the site-specific transport of nanoparticles and to estimate the kinetic coefficients describing these phenomena. Particle transport can be simulated in 1D geometry accounting for relevant field and injection conditions (variable ionic strength, presence of non-Newtonian carrier fluid, etc.). Finally, the radial simulation tool can be used to upscale the laboratory results to more relevant and representative field conditions and have a preliminary estimation of the particle travel distance during the injection.

The numerical code MNM3D was developed to simulate the micro- and nanoparticle transport in 3D domains. The module can predict the retarded transport of micro- and nanoparticles in groundwater and their physico-chemical interaction with the solid matrix. The model can simulate both spatial and temporal distribution of the colloidal particles, accounting for simultaneous dependency of the attachment and detachment kinetics on the groundwater ionic strength and velocity. It can be applied either for short term evaluation of NP distribution around one or more wells, such as in case of groundwater remediation via engineered NP injection (velocity dependent coefficients), and long term particle spreading prediction, e.g. fate of NP release from a landfill (ionic strength dependent coefficients).

The tool was validated against experimental data and other consolidated numerical tools, namely MNMs, providing always satisfactory results. With respect to the other available simulation tools for nanoparticles transport, MNM3D can be applied to more realistic domains, with complex geometries and boundary conditions. Inhomogeneity of the porous medium and of the particle-soil interactions can be taken into account by implementing space-variable hydrodynamic, transport and kinetic parameters. Moreover, MNM3D can be easily implemented in many open-source and commercial graphical interface which already support the well-known RT3D numerical code it is based on. Therefore, MNM3D overcomes many limitations and approximations of the other simplified numerical codes and offers the opportunity to fill the gap between the controlled conditions of laboratory tests and the more complex scenarios typical of field-scale applications. If coupled with MNMs, MNM3D can be used at the final stage of the remediation design process, as a support to estimate important operative parameters, including particle distribution around the injection well, influence radius for a target concentration, number of required injection wells, etc.

4 Using the modelling tools to assist NP-based remediation

4.1 Getting the software

The macro-scale modelling tools are intended for practical support in the design and interpretation of an NP-based remediation. The pore scale NanoPNM model is a research tool that was used in support of the development of the macro-scale module. Those interested in using NanoPNM for further research should contact co-author Amir Raouf.

MNMs can be downloaded from the Polito website (<http://www.polito.it/groundwater/software>), where also step by step tutorials and example files can be found. MNM3D is a modified version of the well-known transport model RT3D (Clement, 1997, Clement et al., 1998) in which the colloid transport equations and the coupled dependencies of attachment and detachment kinetic coefficients on transients in pore water ionic strength and velocity have been implemented. MNM3D can be easily implemented in many open-source and commercial graphical interfaces which already support RT3D, like Visual Modflow. MNM3D is currently being implemented in Visual Modflow (Waterloo Hydrogeologic) and will be included as a transport simulation package in the next release of the software in 2017. A detailed description of MNM3D and two examples of its application are provided in Bianco et al. (2016).

4.2 Limiting the number of tests to be performed in the laboratory

As discussed above, several parameters have a significant effect on the overall mobility of the NPs injected at the site. Those expected to play a major role in the field-scale mobility of the NPs should be identified. As an example, if the aim of the column tests is to gather information for a pilot injection through a screened well, then flow velocity is expected to be a key parameter to be investigated. As a consequence, few (typically three or four) column tests will be run injecting particles at different flow rates. If the parameter of interest is the injected concentration, or the concentration of stabilizer, the same approach can be adopted, running few column tests at different NP or stabilizer concentration. MNMs is then applied to extract quantitative information on the key transport features associated with the investigated parameter (inverse mode), and also to simulate NP transport under a wider set of conditions (forward mode). The latter helps to identify which range of conditions should be covered by the column experiments. Modelling may thus spare extensive cost- and time-consuming experiments, while widening the range of conditions that can be investigated.

4.3 Exploring different implementation scenarios

The information gathered from the modelling of the column tests, in terms of processes identified and associated rate parameters, has general validity and can thus be extended to more complex scenarios. In this case simulations are run in forward mode, to forecast NP transport under various implementation scenarios, and the model results can aid in optimizing NP and slurry properties and injections schemes (e.g. based on a desired radius of influence and NP concentration in the target area, which discharge rate should be applied, how long injection should last, which concentration of NPs and stabilizers is the most effective, ...). Equally important, model results can point out what

crucial but still missing information would contribute most to making a better-informed decision, and therefore suggest if and which additional laboratory transport tests should be performed to fill knowledge gaps.

4.4 Guiding monitoring and testing assumptions

Model forecasting should always go hand in hand with adequate monitoring and vice versa. Model results can guide how, where and when to monitor, to proof that the expectations on NP placement - and remediation targets and safety – will be met. Model forecasts that cannot be verified are useless, as are monitoring data that cannot be tested against prior expectations. Any discrepancy between actual observation and previous prediction should be reason to question and revise aspects of the conceptual site model and to adjust any follow-up activities accordingly.

4.5 Overall strategy

As an example, Figure 17 depicts the various steps - combining experiments, modelling, and monitoring - that could be followed in the model-assisted design of a pilot injection of NPs through a screened well for the case of a fairly homogenous aquifer system:

- NP slurry and porous medium are characterized in detail;
- Columns are packed using the site porous medium, and a tracer test is run on each column to determine porosity and dispersivity;
- Few transport tests under well-defined conditions are performed at different injection rates (typically three or four);
- Based on NP and porous medium properties, a first guess of the transport-controlling mechanisms is made (e.g. data indicate that ripening can be assumed);
- Transport coefficients (k and f parameters of eq. 1-2) are fitted against experimental results; if model fitting is unsatisfactory, the initial guess on transport mechanisms is updated via an iterative procedure (e.g. comparison of model and experimental data suggest that physical filtration may dominate over blocking);
- The trend of k_{att} and k_{det} with flow velocity and/or other underlying factors is verified against the theoretical model formulation used (see the Appendix for details on the mathematical formulations), and the values of the underlying coefficients are determined;
- 1D- radial simulations are run in forward mode assuming the transport mechanisms and parameters as determined in the previous steps. Several radial simulations can be run, e.g. assuming different injection rates, or different injection durations, thus deriving the expected radius of influence, particle spatial distribution and associated pressure build-up for each set of operative conditions (see Tosco et al., 2014, for an example of application).
- Based on the model results, the preferred injection scenario for the pilot test is implemented.

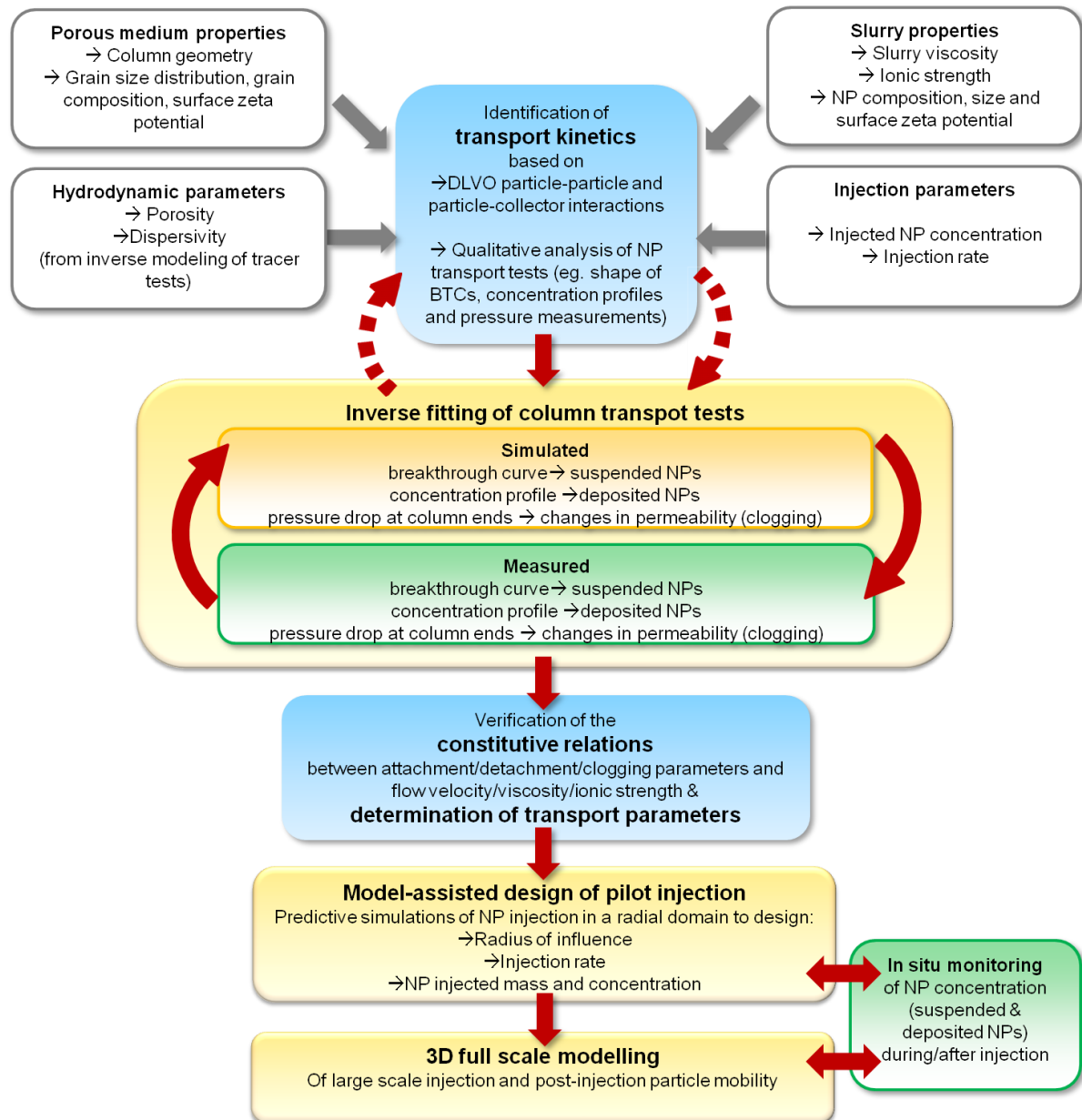


Figure 17: Procedure for the interpretation of column transport tests to derive information for the simulation at larger scales

- After the pilot test is performed, the particle distribution around the injection point and radius of influence predicted by the model are compared to those obtained in the field. To this aim, monitoring results collected during the pilot injection and after are needed. In particular, it is crucial to have information on the NP mobility during the injection (which can be obtained, for example, by collecting water samples over time in monitoring piezometers around the injection point), and the final particle distribution after injection (to be reconstructed, for example by analysing the concentration of NPs in soil cores collected in the proximity to the injection point, at various distances).
- If the model and experimental results of the pilot injection are in good agreement, then the model is validated, and the transport mechanisms and coefficients derived from the laboratory tests can be assumed valid also at the large (field) scale. If the agreement is not satisfac-

tory, the model parameters are adjusted in order to match the pilot monitoring results, and the new set of parameters is used for further steps of the remediation design (e.g. for modelling the full scale injection of NPs).

A similar procedure applies in case the radial domain considered in MNMs is an oversimplification, and a full 3D modelling tool (i.e. MNM3D) is to be used. Examples are the design of a pilot injection in a strongly heterogeneous medium, or in the presence of a strong background natural flow. Also in this case the 1D model is to be run in inverse mode to derive the transport-controlling parameters from column tests and the full 3D model in predictive mode to explore the possible range of scenarios.

Other examples where a full 3D model is called for are the full scale design of a field injection in a heterogeneous aquifer with multiple wells or to forecast the NP mobility on a longer time frame. Here, specifically the modelling-monitoring feedback system can be used to guide an adaptive remediation strategy.

5 Large scale modelling results

5.1 Carbo-Iron® injection in the small flume experiment

A Carbo-Iron® nanoparticle suspension (SciDre GmbH, UFZ Leipzig) was injected in a 2D pilot scale flume (Bleyl et al. 2012, Mackenzie et al. 2012, Giannelli et al. 2014, Giannelli et al. 2015) carried out at the VEGAS facility (VEGAS, USTUTT). A container of 1.0x0.12x0.7 m (LxWxH) filled with homogeneous quartz sand (Dorfner, Germany) simulating a confined aquifer was used for the injection (Figure 18). A suspension of Carbo-Iron® particles at a concentration $C_{CI}=20$ g/l, stabilized by addition of Carboxymethyl cellulose (CMC, $C_{CMC}=4$ g/l) was injected in the central part of the domain through 4 delivery points for 48 minutes (Figure 19).

The Carbo-Iron® injection was then simulated using MNM3D in order to check the capability of the code in complex and more realistic conditions. The inverse modelling of column transport tests performed before the 2D injection indicated that Carbo-Iron® retention onto the sand can be modelled assuming a single-site interaction with linear reversible attachment. The simulated maps of total particle concentration (retained and suspended particles) were compared to the images of the flume after 7 and 34 mins of NP injection (Figure 19). The simulated contour line corresponding to a total concentration of Carbo-Iron® nanoparticles equal to 7 g/l (white line in Figure 19 C-D-E-F) was chosen to reproduce the edge of the plume (black) visible through the glass wall of the container (Figure 19A-B). Figure 19A-B reports the experimental results after 7 and 34 minutes of injection. In Figure 19C-D they are compared to the simulated plumes of Carbo-Iron®, while in Figure 19E-F a comparison with a simulated injection of a tracer in the same operative conditions is shown. Refer to Bianco et al. (2016) for additional information.

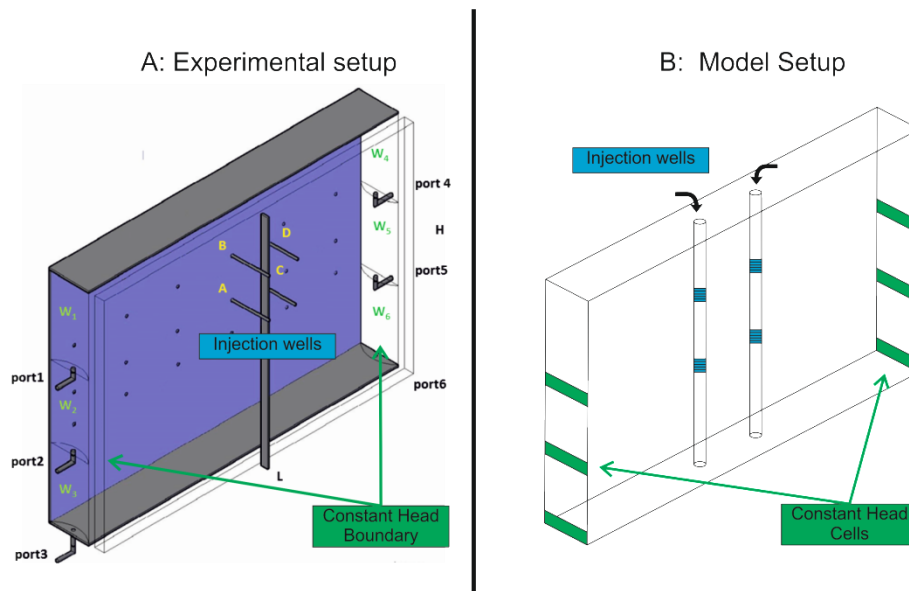


Figure 18: Front view of the large scale flume. Experimental setup (A) and model (B).

The velocity-dependent attachment implemented in MNM3D reproduces well the experimental plume, catching the shape of the experimental spreading area. The partial asymmetry observed in

the experimental data is due to a slightly higher injection rate associated to the injection points located in the left part of the flume. Compared to the tracer simulation results, MNM3D better reproduces the particle behaviour both in terms of spreading area, which is overestimated in Figure 19E-F, and expected concentration distribution. The retarded transport of the Carbo-Iron® particles is due to the interaction with the porous medium.

The overall good quality of the matching between experimental and modelled plume, suggests that MNM3D can correctly describe the transport of Carbo-Iron® in 2D domains in the presence of strong spatial variations of flow velocity.

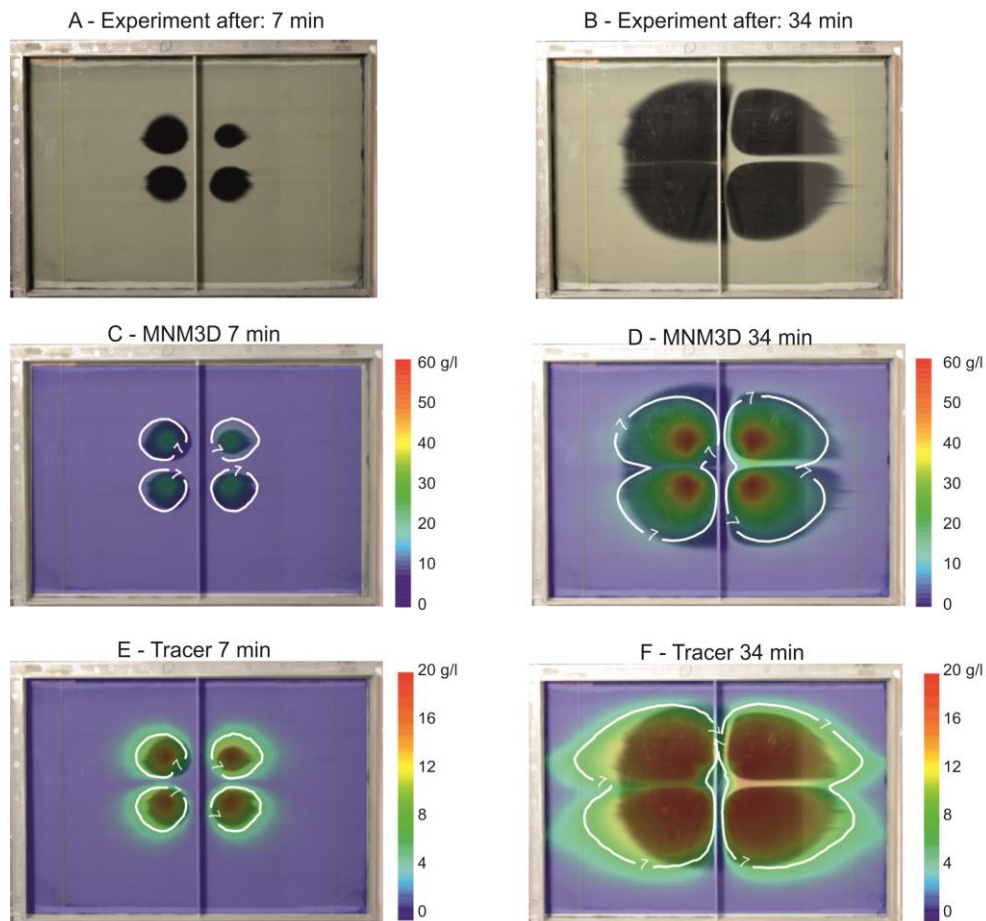


Figure 19: Spreading area of Carbo-Iron® concentration (front view, experiment carried out at VEGAS) after 7 (A) and 34 (B) minutes from the start of the particle injection. Visual comparison between experimental (black plume) and simulated (colored) results of nanoparticle transport (C, D) and tracer transport (E, F) (Bianco et al. 2016).

5.2 Carbo-Iron® injection in the large scale flume experiment

Carbo-Iron® (SciDre GmbH, UFZ Leipzig) was also injected in the large scale flume (LSF) experiment (VEGAS, USTUTT). The LSF is a tank 6x1x3 m (L x W x H) large filled with homogeneous quartz sand (Dorfner, Germany) and simulating an unconfined aquifer (Figure 20). A suspension of Carbo-Iron® particles at a concentration $C_{CI}=20$ g/L was injected twice in the central part of the domain through a single well to generate a near-well emplacement of the Carbo-Iron®. Two injections were performed using two different concentrations of CMC as stabilizer. The first injection was carried out at 1 g/L of

CMC and lasted around 80 min, while in the second one the particles were injected for around 160 min at a 2 g/L concentration of stabilizer. The total injection time was of around 4 hours. The shape of Carbo-Iron® plume was visually analysed through the glass walls of the tank (Figure 21) and core samples were collected after injection at several points and at different depths of the container and the iron content analysed.

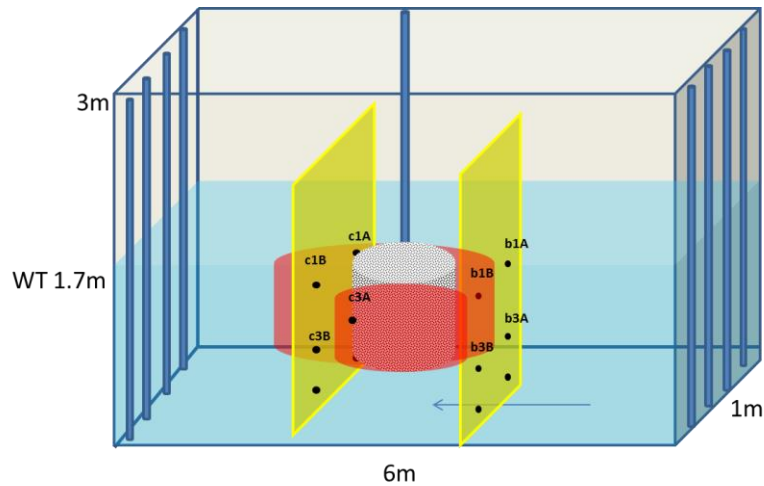


Figure 20: Conceptual model of the Large Scale Flume Experiment

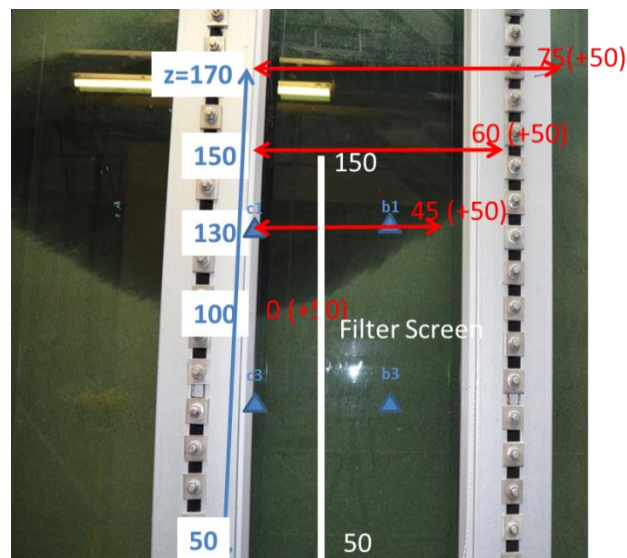


Figure 21: Visual analysis of the Carbo-Iron® plume through the glass wall of the tank

The injection of Carbo-Iron® particles in the LSF was simulated using MNM3D. A single 4-hour-long injection was here considered. The injection well was located at $x = 2.5$ m (Figure 22). The kinetic coefficients governing the transport of Carbo-Iron® in the same quartz sand used to fill the tank were determined by inverse fitting of a cascading column experiment carried out at VEGAS. Cascading column experiments consist of a set of column tests carried out at different decreasing velocities to simulate the transport of particles during injection. A particle suspension is first injected in a sand-packed column at high discharge rate, mimicking the near well conditions. The suspension collected at the first column outlet is then injected in a second column using a lower discharge rate, which

simulates the transport of the particles at a longer distance from the injection well. The procedure can be repeated with any number of columns and decreasing velocities. A schematic representation of a cascading column test is shown in Figure 23a. The cascading column test carried out at VEGAS involved only two columns. The main properties of the columns and the operating conditions of the test are reported in Table 7. The experimental breakthrough curves were interpreted using MNMs (Figure 23b-c). The data fitting results evidenced no significant dependency of the deposition kinetics on the pore water velocity, resulting in a constant attachment coefficient of $1.35 \cdot 10^{-4} \text{ s}^{-1}$.

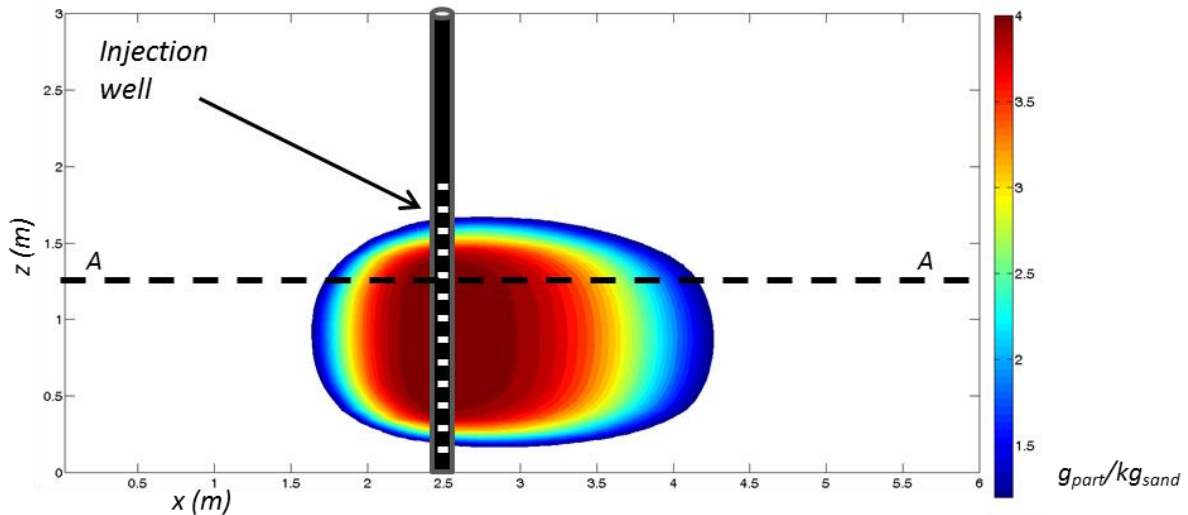


Figure 22: Simulation of Carbo-Iron® injection in the large scale flume: vertical section. The injection well is located at $x = 2.5 \text{ m}$ from the left of the tank. The section A-A indicates the distance from the bottom of the tank at which the simulation results and the core sample analysis are compared in Figure 25.

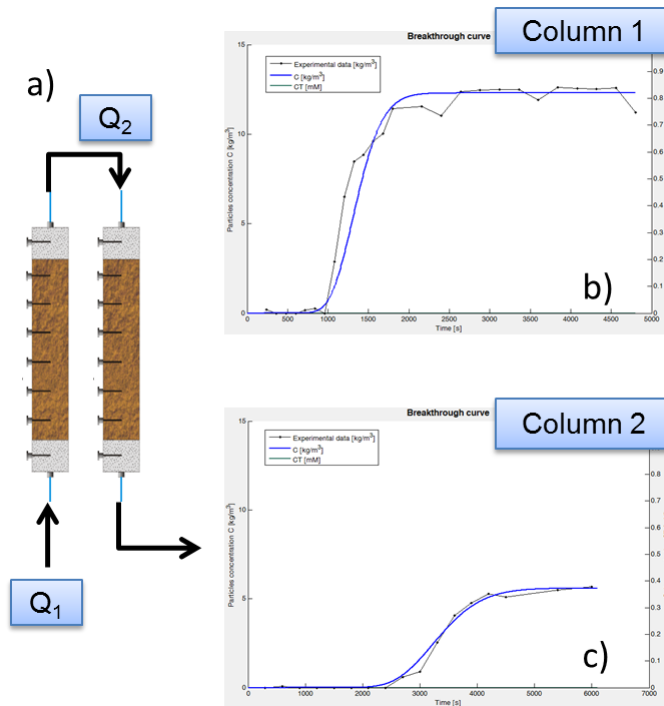


Figure 23: Cascading column test: a) schematic representation of the test; b) and c) fitting of the breakthrough curves obtained by measuring the outlet concentration of the first and second column respectively

Table 7: Properties of the setup and operating conditions of the cascading column experiment carried out at VEGAS

	Column 1	Column 2
Length [cm]	25	
Diameter [cm]	4.4	
Porosity	0.34	
Dispersivity [m]	0.0039	
Q [ml/min]	5.7	2.3
Inlet concentration [g/l]	14.8	8.75

The total concentration distribution (particles in liquid phase + particles in solid phase) in the LSF (vertical section) at the end of the MNM3D simulation is shown in Figure 22. The edge of the simulated plume reported in Figure 22 corresponds to a total iron concentration of 1.2 g/kg, which was identified as the limit concentration which can be visually observed in the flume experiments. Comparing Figure 21 and Figure 22, shows that MNM3D reproduced well the shape and size of the experimental plume: the radius of influence (ROI) of the simulated injection was comparable with the experimental ROI, which was found to be around 70 cm. Moreover, the simulation shows that a large amount of particles was deposited in the proximity of the injection well, confirming that the desired near-well distribution of the Carbo-Iron[®], which was the main goal of the experiment, was achieved.

The spatial distribution of the total NP concentration was determined by analysis of core samples collected after the injection. The map of total particle concentration (top view of the LSF) simulated in MNM3D at 1.3 m from the bottom of the tank and the position of the core sampling is reported in Figure 24. Table 8 reports the Carbo-Iron[®] concentration measured in the core samples (derived from TOC analysis of the carbon) and the corresponding MNM3D simulation results.

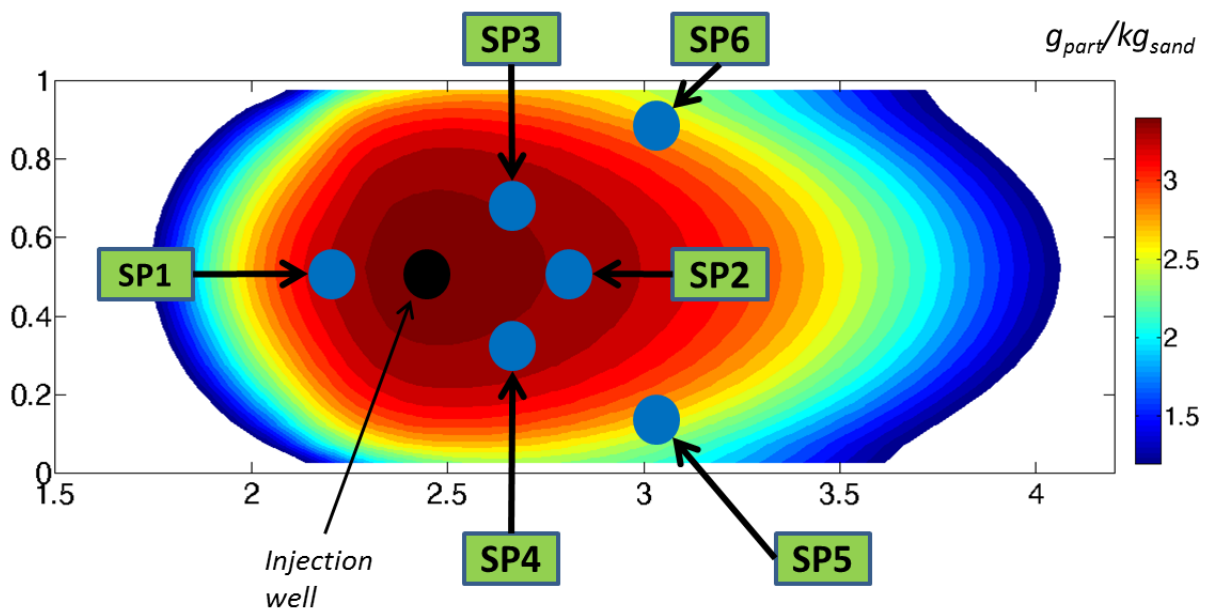


Figure 24: Simulation of Carbo-Iron[®] injection (view from the top) and position of the core sampling. Zoom on the injection area at 1.3 m from the bottom of the tank.

Table 8: Comparison of measured (derived from TOC analysis) and simulated concentration at the core sampling points at a distance of 1.3 m from the bottom of the tank.

Monitoring point		Observed concentration	Model results
SP 1	g/kg	3.40	3.39
SP 2	g/kg	3.30	3.43
SP 3	g/kg	2.20	3.39
SP 4	g/kg	3.30	3.39
SP 5	g/kg	4.90	3.19
SP 6	g/kg	NO data	3.05

Very good agreement was found between simulated and experimental results, proving that MNM3D can capture and reproduce the transport behaviour of the Carbo-Iron[®] particles in complex geometries. Moreover, the good results obtained using kinetic coefficients directly estimated by data fitting of cascading column experiments, without further adjustments against LSF results, demonstrates that the upscaling procedure is robust. This approach, including the coupled use of column experiments, MNMs data fitting and MNM3D simulations, may therefore be applied to predict the migration of Carbo-Iron[®] particles at larger scales.

5.3 Carbo-Iron[®] injection at Balassagyarmat

A field test with injection of Carbo-Iron[®] (SciDre GmbH, UFZ Leipzig) was performed at the Balassagyarmat site, Hungary (Golder). The pilot injection was performed through three injection points at 3 m distance each. In total 180 kg of Carbo-Iron[®] were injected at a concentration of 15 g/L. The suspension was stabilized with addition of 1.5 g/L of CMC. The injection lasted for approximately 3 hours and was performed at a flow rate of 20 l/min. A background groundwater flow of 2 m/d was simulated. Core samples were taken at a distance of 0.5, 1 and 1.7 m from the wells (Figure 25).

Table 9 reports details about the positions of the core samples and the concentration of Carbo-Iron[®] particles detected. The test injection site was modelled as a heterogeneous aquifer (Figure 26), whose parameters were derived from a large scale numerical model (modelled area of 250 x 450 m), developed before NanoRem, and provided by Golder. The model was locally refined to get a reliable simulation of the injection and transport of nanoparticles at the test site.

Table 9: TOC analyses of soil samples from field site for estimation of particle fate

Core / Sample port	Distance to injection well L [m]	Layer bgl [m]	TOC [wt-%]	Particle mass loading [wt-%]*
CMT 7	1.7m (between I3 and I2)	13.3	0.04	0.08
CMT 8	1m (downstream to I2)	13.5	0.09	0.2
CMT 9	0.5 (downstream to I3)	13.8	0.13	0.3
CMT 9	0.5 (downstream to I3)	13.3	0.18	0.4

* sediment loading estimated from TOC and assuming 50% carbon content in Carbo-Iron[®]

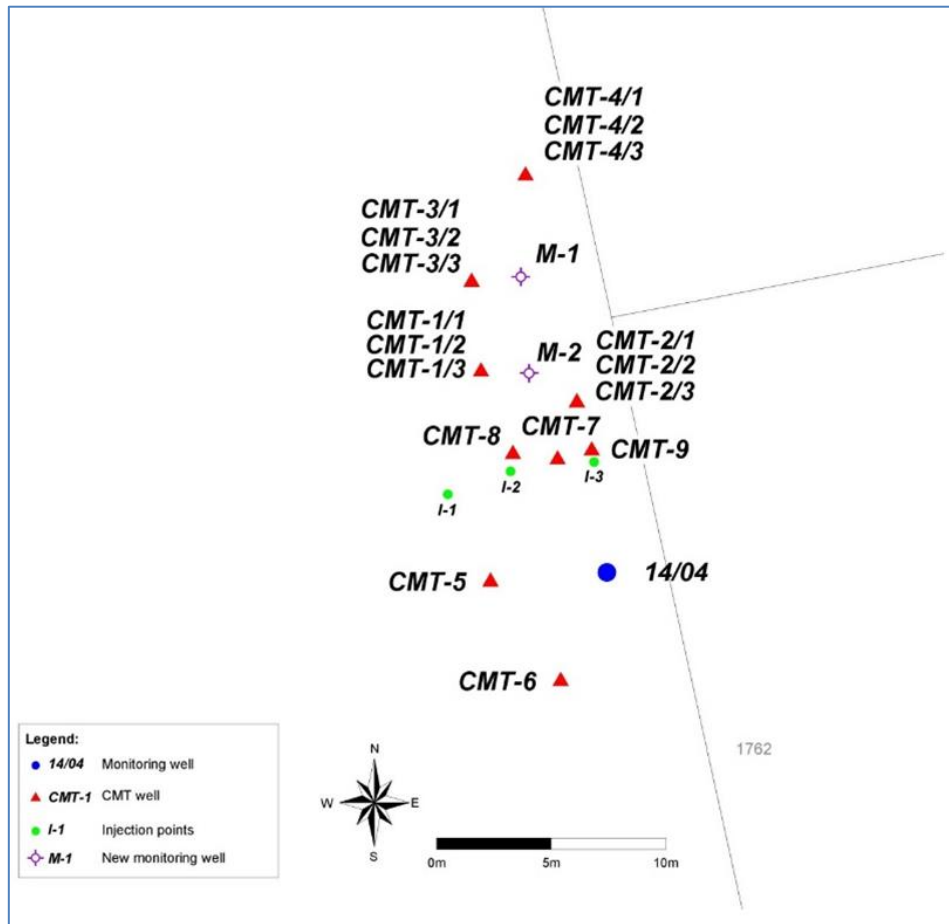


Figure 25: Location of injection (I-1, I-2, I-3) and monitoring points (CMT-7, CMT-8, CMT-9)

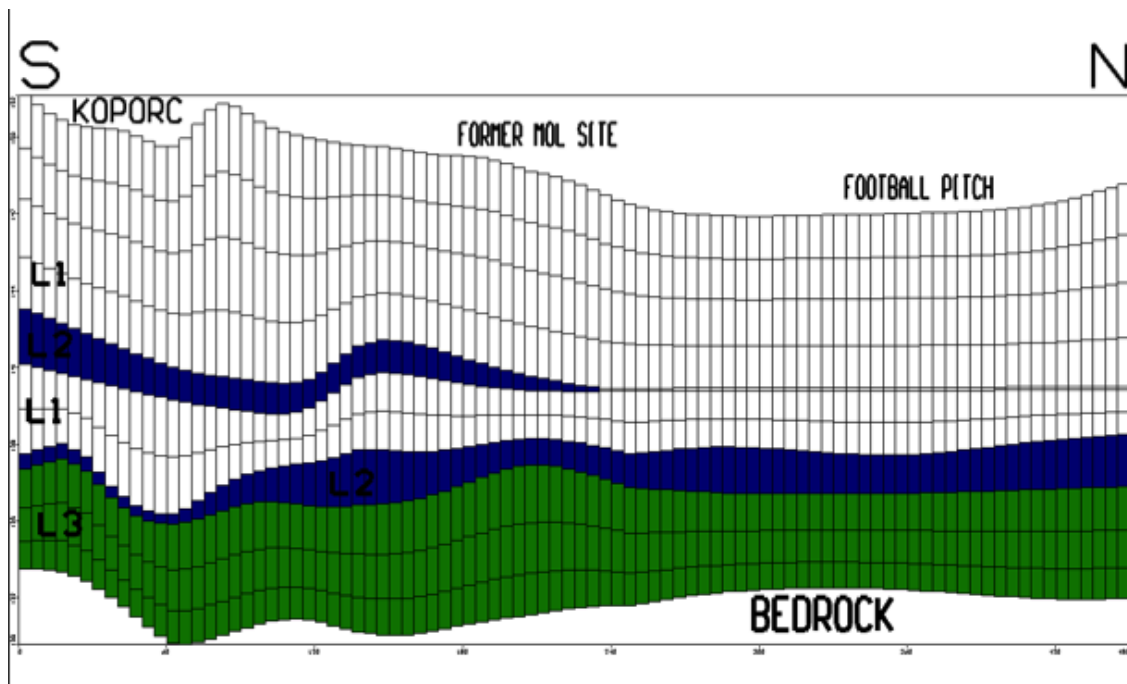


Figure 26: Large scale model (section view) of the Balassagyarmat site provided by Golder before the refinement of the grid as required for NP transport simulation. Green represents the high permeability layer where NPs were injected.

The kinetics of NP transport in porous media are site-specific (dependency on particles type, porous medium properties, dispersant, etc.) and some fitting parameters have to be estimated from column tests in order to run a reliable MNM3D simulation. As a consequence, the attachment/detachment kinetics used for the simulation of the small and large scale flumes cannot be directly applied to the simulation of the field test, since the porous medium where the particles are injected is different.

The NP injection at the site was simulated in MNM3D assuming that particle deposition was controlled by linear reversible attachment, with attachment kinetics k_{att} dependent on the pore water velocity (eq. 3-4), as evidenced in previous works (Tosco et al. 2014b). In the work plan, the kinetic coefficients of eq. 3-4 were supposed to be estimated by column tests performed using sand collected from the site and injecting particles at different flow rates, thus following the procedure described in Chapter 4. However, only one column test (seepage velocity of 10 m/d) was available at the end of the project. As a consequence, a value of attachment and detachment rate was estimated by fitting the results of the column test available at the moment, and the dependence of attachment and detachment rate expressed by eq. 3-4 was assumed valid, thus determining the function relating attachment and detachment rate and flow velocity. The estimated coefficients are reported in Table 10, the experimental breakthrough curve fitted using MNMs is reported in Figure 27.

Table 10: Kinetic coefficients estimated by Carbo-Iron® column test carried out by UFZ. Porous medium from core samples from the Balassagyarmat site.

Parameter		Value
$K_{att,1}$	$[s^{-1}]$	$3.29 \cdot 10^{-2}$
$K_{det,1}$	$[s^{-1}]$	$7.15 \cdot 10^{-2}$
$K_{att,2}$	$[s^{-1}]$	$1.24 \cdot 10^{-4}$

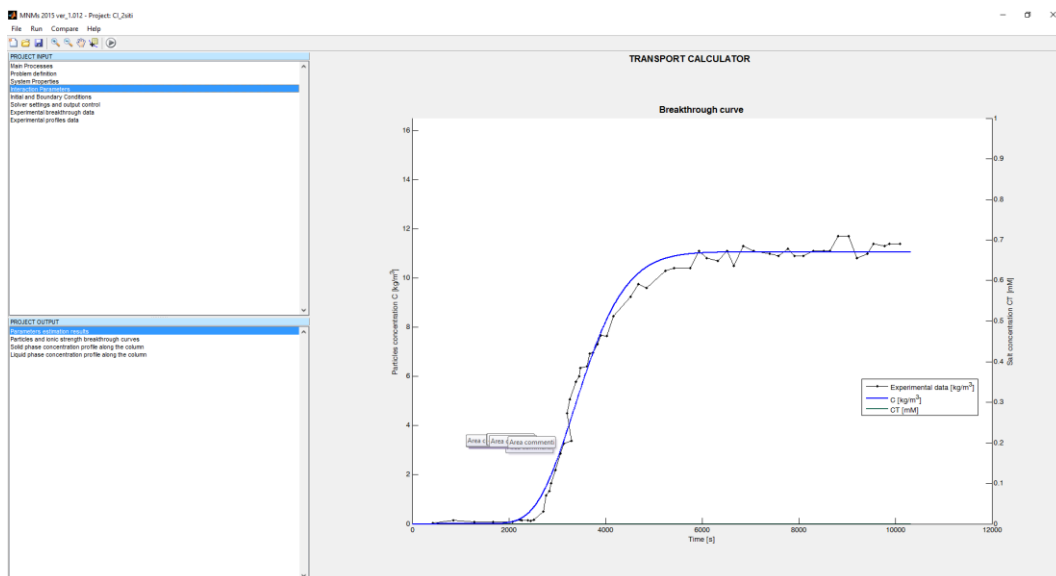


Figure 27: Interpretation of Carbo-Iron® transport test using MNMs. Experimental data from UFZ.

The results of the large scale transport simulation obtained from MNM3D, using the kinetic coefficients determined from the column test, are reported in Figure 28 showing the concentration of particles deposited in the solid phase (g of particles per kg of soil). The simulation showed a useful radius of influence of around 5 m. A particle concentration of 0.8 g/kg was obtained in CMT-7, in line with the concentration measured in the appropriate core sample. The simulated concentrations in the other monitoring points were instead in the order of 1 g/kg. This is quite close to the measured values (between 2 and 4 g/kg), in particular considering all the uncertainties related to the field operation, e.g. the injected concentration and the injection flow rate which are difficult to be kept constant, and to the estimation of the kinetic coefficients (based on one single column test).

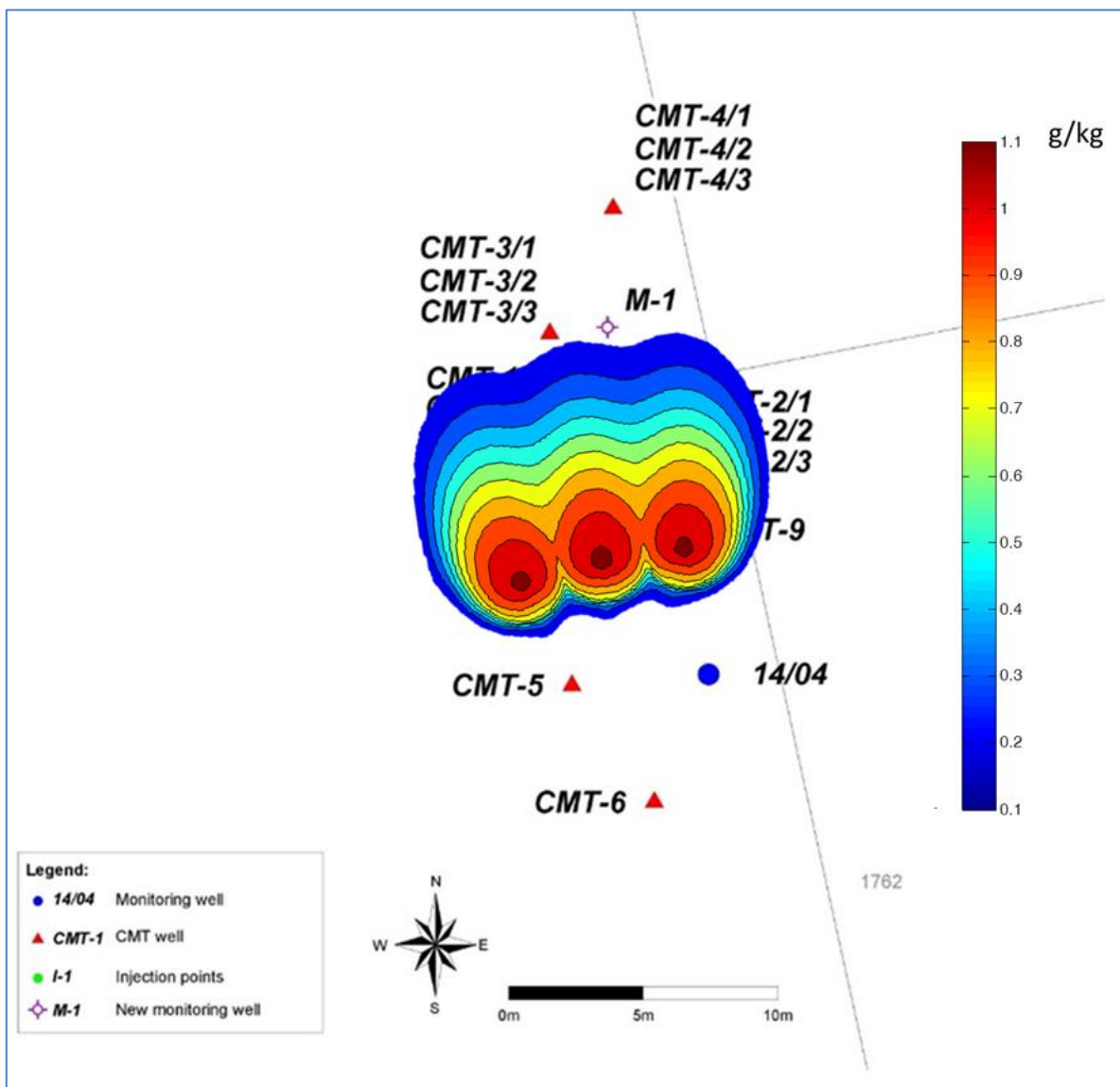


Figure 28: MNM3D simulation of Carbo-Iron® concentration after 9 h of injection at 25 l/min.

6 Conclusions

6.1 Pore scale modelling

A pore-network was developed and applied to relate macro-scale sorption parameters to the underlying pore-scale variables such as solution pH and ionic strength, zeta potential of nanoparticles and grains, nanoparticle sizes, pore sizes, and water flow velocity. However, implementing fundamental single pore scale relationships based on these parameters, the pore-network model showed less attachment of nano-particles than observed in laboratory scale column experiments. Also, observed patterns of NP attachment - occurring already close to column inlets - and observed ionic strength dependencies could not be explained with the fundamental relations available. It is therefore concluded that the above mentioned variables are insufficient predictors for colloid retention under environmental conditions. Additional factors, like grain surface roughness, surface chemical heterogeneity, and particle-particle interaction, contribute to the observed enhanced NP adsorption.

The tracer simulations performed with the pore network highlighted the importance of considering the representativity of packed laboratory columns for the field situation. Laboratory tests should ideally be performed on undisturbed columns and NP breakthrough tests should always be combined with a tracer test for the exact same column.

6.2 Macro scale modelling

Two numerical codes were developed in NanoRem for the macro scale simulation of injection and transport of nanoparticles in groundwater:

- **MNMs** is a Matlab-based numerical code with a user friendly graphical interface for the simulation of nanoparticle transport at the laboratory and pilot scale. MNMs can be used for interpretation of column tests accounting for the influence of several parameters (e.g. ionic strength, carrier fluid viscosity, clogging, etc.) and for the preliminary characterization nanoparticle suspensions (DLVO interaction profiles and single collector efficiency calculation). MNMs can be also used to simulate the injection of nanoparticles in a homogeneous aquifer through a single well, assuming a 1D radial symmetry of the domain. This is a useful tool for the preliminary optimization of pilot injections in the framework of a nanoremediation design.
- **MNM3D** is a full 3D numerical code for the simulation of the velocity and ionic strength dependent transport of nanoparticles in complex aquifer systems. MNM3D can account for heterogeneity of the porous media, generic boundary conditions and complex background natural flow. It was developed as a support tool for the design of full scale nanoremediation and to assess the long term behaviour of nanoparticles after injection. The code is currently being implemented in the Visual Modflow graphical interface, and will be included as a transport simulation package in the next release of Visual Modflow in 2017. This will make it easily available to practitioners and consultants and promote its diffusion in the remediation field.

MNMs and MNM3D proved to be useful tools at different stages of a nanoremediation design. Coupled together, they represent a robust toolbox for the characterization of nanoparticle transport, the interpretation of column tests, the upscaling of the derived correlations and the final application to the design of a full scale nanoremediation.

List of References

- Bianco, C., Tosco, T. and Sethi, R. (2016) A 3-dimensional micro- and nanoparticle transport and filtration model (MNM3D) applied to the migration of carbon-based nanomaterials in porous media. *Journal of Contaminant Hydrology* 193, 10-20.
- Bleyl, S., Kopinke, F.D. and Mackenzie, K. (2012) Carbo-Iron[®]-Synthesis and stabilization of Fe(0)-doped colloidal activated carbon for in situ groundwater treatment. *Chemical Engineering Journal* 191, 588-595.
- Clement, T.P. (1997) A Modular Computer Code for Simulating Reactive Multi-species Transport in 3-Dimensional Groundwater Systems. Pacific Northwest National Laboratory, U.S.D.o.E. (ed), Auburn, Alabama.
- Clement, T. P., Sun, Y., Hooker, B. S. & Petersen, J. N. (1998) Modeling multispecies reactive transport in ground water. *Ground Water Monit. Rem.*, 18, p. 79-92
- Crevacore, E., Tosco, T., Sethi, R., Boccardo, G., Marcisio, D. (in press) Recirculation zones induce non-Fickian transport in 3D periodic porous media. *Physical Review E*.
- Giannelli, G., Bleyl, S., Sethi, R. and Braun, J. (2015) Small Flume Experiment for the Transport Evaluation of CARBO-IRON[®] particles in a confined aquifer, Copenhagen.
- Giannelli, G., Sethi, R. and Braun, J. (2014) Small Flume Experiment for the Transport Evaluation of Carbo-Iron Particles in a Confined Aquifer, Darmstadt.
- Hofmann, T., Wagner, S., Velimirovic, M., Micic Batka, V. and Schmid, D. (2015) Report on the stability, mobility, and enhanced delivery of NPs, for NPs that are accessible at the beginning of the project: IDL-4.2. NanoRem FP 7 Project GA No 309517. www.nanorem.eu
- Mackenzie, K., Bleyl, S., Georgi, A. and Kopinke, F.D. (2012) Carbo-Iron - An Fe/AC composite - As alternative to nano-iron for groundwater treatment. *Water Research* 46(12), 3817-3826.
- Messina, F., Marchisio, D.L. and Sethi, R. (2015) An extended and total flux normalized correlation equation for predicting single-collector efficiency. *Journal of Colloid and Interface Science* 446, 185-193.
- Messina, F., Tosco, T., Sethi, R. (2016) On the failure of upscaling the single-collector efficiency to the transport of colloids in an array of collectors. *Water Resources Research* 52 (7), 5492-5505.
- Micić Batka, V., et al. (2016) Stability, Mobility, Delivery and Fate of optimized NPs under Field Relevant Conditions: DL 4.2. NanoRem FP 7 Project GA No 309517. www.nanorem.eu.
- Rajagopalan, R, Tien, C. (1976) Trajectory analysis of deep-bed filtration with the sphere-in-cell porous media model. *AiChE Journal* 22(3), 523-533.
- Raof, A., & Hassanizadeh, S. M. (2010). A new method for generating pore-network models of porous media. *Transport in porous media*, 81, p.391-407.
- Raof, A., Hassanizadeh, S. M., & Leijnse, A. (2010). Upscaling transport of adsorbing solutes in porous media: pore-network modeling. *Vadose Zone Journal*, 9, p.624-636.
- Raof, A., Nick, H. M., Hassanizadeh, S. M., & Spiers, C. J. (2013). PoreFlow: A complex pore-network model for simulation of reactive transport in variably saturated porous media. *Computers & Geosciences*, 61, p.160-174.
- Redman, J. A., Walker, S. L., & Elimelech, M. (2004). Bacterial adhesion and transport in porous media: Role of the secondary energy minimum. *Environmental Science & Technology*, 38(6), 1777-1785.
- Seetha, N., Kumar, M. M., Hassanizadeh, S. M., & Raof, A. (2014). Virus-sized colloid transport in a single pore: Model development and sensitivity analysis. *Journal of contaminant hydrology*, 164, p.163-180.
- Seetha, N., Majid Hassanizadeh, S., Kumar, M., & Raof, A. (2015). Correlation equations for average deposition rate coefficients of nanoparticles in a cylindrical pore. *Water Resources Research*, 51(10), 8034-8059.
- Šimůnek, J., Van Genuchten, M.T. and Šejna, M. (2008) Development and applications of the HYDRUS and STANMOD software packages and related codes. *Vadose Zone Journal* 7(2), 587-600.
- Tufenkji, N., Elimelech, N. (2004) Correlation Equation for Predicting Single-Collector Efficiency in Physicochemical Filtration in Saturated Porous Media. *Environmental Science & Technology* 38(2), 529-536.
- Tosco, T., Bosch, J., Meckenstock, R.U. and Sethi, R. (2012) Transport of ferrihydrite nanoparticles in saturated porous media: Role of ionic strength and flow rate. *Environmental Science and Technology* 46(7), 4008-4015.
- Tosco, T., Gastone, F. and Sethi, R. (2014a) Guar gum solutions for improved delivery of iron particles in porous media (Part 2): Iron transport tests and modeling in radial geometry. *Journal of Contaminant Hydrology* 166(0), 34-51.

- Tosco, T., Gastone, F. and Sethi, R. (2014b) Guar gum solutions for improved delivery of iron particles in porous media (Part 2): Iron transport tests and modeling in radial geometry. *Journal of Contaminant Hydrology* 166, 34-51.
- Tosco, T., Petrangeli Papini, M., Cruz Viggi, C. and Sethi, R. (2014c) Nanoscale iron particles for groundwater remediation: a review. *Journal of Cleaner Production* 77, 10-21.
- Tosco, T. and Sethi, R. (2009) MNM1D: a numerical code for colloid transport in porous media: implementation and validation. *American Journal of Environmental Sciences* 5(4), 517-525.
- Tosco, T. and Sethi, R. (2010) Transport of non-newtonian suspensions of highly concentrated micro- and nanoscale iron particles in porous media: A modeling approach. *Environmental Science and Technology* 44(23), 9062-9068.
- Tosco, T., Tiraferri, A. and Sethi, R. (2009) Ionic Strength Dependent Transport of Microparticles in Saturated Porous Media: Modeling Mobilization and Immobilization Phenomena under Transient Chemical Conditions. *Environmental Science & Technology* 43(12), 4425-4431.
- Yao, K.-M., Habibian, M.T. and O'Melia, C.R. (1971) Water and waste water filtration. Concepts and applications. *Environmental Science & Technology* 5(11), 1105-1112